© 2022. Published by The Company of Biologists Ltd | Development (2022) 149, dev200549. doi:10.1242/dev.200549

RESEARCH ARTICLE

Sex-biased effects on hippocampal circuit development by perinatal SERT expression in CA3 pyramidal neurons

Roberto De Gregorio[1], Galadu Subah[2,*], Jennifer C. Chan[3,*,‡], Luisa Speranza[4], Xiaolei Zhang[2], Aarthi Ramakrishnan[3], Li Shen[3], Ian Maze[3,‡], Patric K. Stanton[2] and Ji Y. Sze[1,§]

ABSTRACT

Neurodevelopmental disorders ranging from autism to intellectual disability display sex-biased prevalence and phenotypical presentations. Despite increasing knowledge about temporospatial cortical map development and genetic variants linked to neurodevelopmental disorders, when and how sex-biased neural circuit derailment may arise in diseased brain remain unknown. Here, we identify in mice that serotonin uptake transporter (SERT) in non-serotonergic neurons – hippocampal and prefrontal pyramidal neurons – confers sex-biased effects specifically during neural circuit development. A set of gradient-patterned CA3 pyramidal neurons transiently express SERT to clear extracellular serotonin, coinciding with hippocampal synaptic circuit establishment. Ablating pyramidal neuron SERT (*SERT*$^{Pyramid\Delta}$) alters dendritic spine developmental trajectory in the hippocampus, and precipitates sex-biased impairments in long-term activity-dependent hippocampal synaptic plasticity and cognitive behaviors. Transcriptomic analyses identify sex-biased alterations in gene sets associated with autism, dendritic spine structure, synaptic function and male-specific enrichment of dysregulated genes in glial cells in early postnatal *SERT*$^{Pyramid\Delta}$ hippocampus. Our data suggest that SERT function in these pyramidal neurons underscores a temporal- and brain region-specific regulation of normal sex-dimorphic circuit development and a source for sex-biased vulnerability to cognitive and behavioral impairments.

This article has an associated 'The people behind the papers' interview.

KEY WORDS: SERT, Trophic serotonin, Circuit assembly, Hippocampus, Sex-biased genetic programming, Sex-biased circuit plasticity

INTRODUCTION

Organismal cognitive capabilities, perception and behaviors are shaped during the development of synaptic circuits. While cell identity, and laminar and area position of cortical neurons are defined during neurogenesis to form stereotyped brain structure, neuronal gene expression patterns and synaptic connectivity are dynamically reconfigured by physiological and environmental cues during functional maturation at their terminal destination to shape circuit properties (Cadwell et al., 2019; Rakic et al., 2009). Alterations in synaptic circuit assembly are believed to be a major source of inter-individual variations in cognitive processing and susceptibilities to neuropsychiatric disorders (Bale et al., 2010; Marin, 2016; Silbereis et al., 2016). Despite abundant knowledge about genomic, molecular and cellular mechanisms driving temporal and spatial cortical map development, little is known about temporal-specific intrinsic regulatory mechanisms of circuit assembly (Cadwell et al., 2019; Geschwind and Rakic, 2013). How neurons of diverse types are coherently assembled into local circuits during normal development and in diseased brain remains unclear.

One profound genetic contributing factor to cognitive processing pattern variations is sex. Most neuropsychiatric disorders display sex differences in prevalence and phenotype presentations (Abel et al., 2010; Maenner et al., 2020; Satterthwaite et al., 2015). A consistent feature of transcriptomics of postmortem brain from subjects diagnosed with autism spectrum disorder (ASD) and schizophrenia is small magnitude alterations of multiple genes involved in discrete cellular functions and biological processes, with little overlap of specific genes altered in males versus females (Hoffman et al., 2022; Velmeshev et al., 2019; Werling et al., 2016). This suggests that males and females may employ distinct sets of genes to fine tune (or perturb) converging cellular processes that confer circuit and behavioral outputs. The classic model is that genetic sexes cause differentiation of the gonads to produce hormones that act directly on developing brain to generate sex dimorphic functions. Emerging evidence suggests that sex differences in cognitive processing may originate, in part, from inherent genomic configurations in the brain (Lenz et al., 2012; McCarthy and Arnold, 2011). An ASD-associated allele of the chromatin-remodeling factor Chd8 confers sex-biased, even opposite, alterations in gene expression and behaviors in mice (Jung et al., 2018). Male but not female carriers of genetic variants in synapse scaffolding protein Shank1 and ryanodine receptor 2 (RyR2) manifest ASD (Lu and Cantor, 2012; Sato et al., 2012). However, no diseased brain may be obtained before diagnosis and most disease-susceptibility genes, such as *Chd8*, *Shank1* and *Ryr2*, are broadly expressed throughout life; how sex differences in neural circuits are established, and when and how sex-biased circuit derailment in diseased brain may arise are currently unknown.

The serotonin uptake transporter (SERT; *Slc6a4*) is the primary mechanism for clearing extracellular serotonin (5-HT), to maintain homeostatic 5-HT signaling in the brain (Hahn and Blakely, 2007). It has long been recognized that the effects of reducing SERT function in development and adulthood differ. Selective 5-HT reuptake inhibitors (SSRIs) are the first line treatment for depression

[1]Department of Molecular Pharmacology, Albert Einstein College of Medicine, Bronx, NY 10461, USA. [2]Department of Cell Biology & Anatomy, New York Medical College, Valhalla, NY 10595, USA. [3]Nash Family Department of Neuroscience, Friedman Brain Institute, Icahn School of Medicine at Mount Sinai, NY 10029, USA. [4]Dominick P. Purpura Department of Neuroscience, Albert Einstein College of Medicine, Bronx, NY 10461, USA.
*These authors contributed equally to this work
‡Howard Hughes Medical Institute

§Author for correspondence (jiying.sze@einsteinmed.edu)

J.Y.S., 0000-0002-3828-9335

Handling Editor: François Guillemot
Received 21 February 2022; Accepted 8 September 2022

Development (2022) 149, dev200549. doi:10.1242/dev.200549

in adults. In contrast, reducing SERT function during development, either by *Slc6a4* variants or SSRIs, increases the risk of neuropsychiatric disorders, including ASD (Canli and Lesch, 2007; Caspi et al., 2010; Garbarino et al., 2019; Gingrich et al., 2017; Glover and Clinton, 2016; Schipper et al., 2019).

Patricia Gaspar and colleagues first demonstrated that, unlike in adult brain where SERT is exclusively expressed in raphe serotonergic neurons, in developing brain SERT is additionally expressed in anatomically defined sets of non-serotonergic neurons (Gaspar et al., 2003). Multiple groups, including ours, have confirmed SERT expression in rodents in specific glutamatergic projection neurons in the thalamus, medial prefrontal cortex (mPFC) and hippocampus from embryonic day (E) 17 to postnatal day (P) 10 (Chen et al., 2015; Hansson et al., 1998; Lebrand et al., 1998). These neurons do not synthesize 5-HT but robustly express SERT and the monoamine degradation enzymes MAOA, MAOB and COMT, suggesting a role for these glutamatergic terminals in clearing extracellular trophic 5-HT (Soiza-Reilly et al., 2019). Human cortex single-cell transcriptomics identify SERT expression in glutamatergic neurons between 12 and 18 post-conception weeks (Nowakowski et al., 2017), a period associated with ASD (Geschwind and Rakic, 2013; Marin, 2016; Silbereis et al., 2016). Many human brain developmental processes in midfetal gestation correspond to the first two postnatal weeks in mice (Willsey et al., 2013; Workman et al., 2013), suggesting that these glutamatergic terminals express SERT to control local 5-HT levels in a defined brain developmental stage. We have developed $SERT^{fl/fl}$ mice and demonstrated that regulation of 5-HT levels by SERT expression in glutamatergic thalamocortical axon (TCA) terminals is essential for normal topographic map establishment in target cortex (Chen et al., 2016, 2015; De Gregorio et al., 2020). The role of SERT in functional circuit development has not yet been elucidated.

Here, we study SERT function during synaptic circuit development in the hippocampus, a brain region essential for cognition and stress responses (Kandel et al., 2014). We show that a set of CA3 pyramidal neurons projecting to the CA3, CA1 and DG intrinsic circuits express SERT specifically in the period of hippocampal synaptic circuit maturation. We developed conditional SERT ablation exclusively in the hippocampal and mPFC pyramidal neurons ($SERT^{Pyramid\Delta}$). This permits the identification of SERT function during hippocampal circuit establishment and the long-lasting impact on adult hippocampal functionality. $SERT^{Pyramid\Delta}$ impaired dendritic spine development and resulted in increased mature spine density on adult CA1 pyramidal neurons, highlighting the origin of the alterations caused by SERT dysfunction and secondary adaptive manifestation. Adult $SERT^{Pyramid\Delta}$ male and female mice displayed shared and distinct deficits in long-term activity-dependent CA3-CA1 synaptic plasticity and behaviors. Transcriptomics analyses revealed sex-biased changes in ASD-associated genes, as well as genes involved in synaptic structure and function in early postnatal $SERT^{Pyramid\Delta}$ hippocampus. These data identify that the temporal-specific SERT expression in glutamatergic terminals during circuit assembly is essential for normal long-term activity-dependent synaptic plasticity in the hippocampus, and disrupting this developmental SERT function is a source of sex-biased cognitive and behavioral impairments.

RESULTS

A perinatal-specific hippocampal SERT-expressing glutamatergic projection network

We first explored the relationship between SERT expression in glutamatergic neurons and hippocampal development, by characterizing temporal and spatial SERT expression in the hippocampus (Fig. 1). *In situ* hybridization showed SERT mRNA specifically in the CA3 in the first 10 postnatal days (Fig. 1A; Fig. S1), consistent with previous observations (Hansson et al., 1998; Lebrand et al., 1998). We confirmed SERT expression in CA3 neurons using SERT immunostaining of a knock-in Cre-dependent tdTomato (tdTom) reporter (Madisen et al., 2010) in $SERT^{Cre/+}$ mice (Narboux-Neme et al., 2008; Zhuang et al., 2005) (Fig. 1B; Fig. S2). Using the robust tdTom reporter as a tool, we observed a gradient patterning of SERT-expressing neurons in the perinatal CA3. $tdTom^+$ CA3 neurons emerged at E17.5, progressively increased in number and grew their axons in the first postnatal week (Fig. 1C). Assessing the percentage of the $tdTom^+$ neurons over DAPI-labeled cell nuclei revealed that SERT is expressed in a subset of CA3 pyramidal neurons, with the number increasing gradually and mostly statistically significant from CA3a towards CA3c throughout the dorsoventral hippocampal axis (Fig. 1D, Table S1). Immunostaining for established neuronal markers further confirmed 95.8±0.22% of the $tdTom^+$ neurons colocalized with the glutamatergic CA3 pyramidal neuron marker Hub but not Ctip2, a CA1 pyramidal neuron marker, or the DG granule cell marker Prox1 (Iwano et al., 2012; Sugiyama et al., 2014) (Fig. S3).

We further characterized CA3 SERT-expressing neuron projections using virus-mediated anterograde tracing. We injected adeno-associated viruses expressing Cre-dependent GFP (AAV1.CAG.Flex.eGFP.WPRE.bGH) unilaterally into the hippocampus of P5 $SERT^{Cre/+}$ mice and traced GFP-expressing neurons and their axonal projections in serial sections of the entire brain at P18. We observed GFP expression in a subset of CA3 pyramidal neurons in the injected hippocampus and their axonal projections innervating the stratum oriens and stratum radiatum of CA3 and CA1 both at the ipsilateral-hippocampus and passing the midline via the commissural pathway to the contralateral hippocampus in males and females (Fig. 1E; n=2 females and 4 males). Consistent with CA3c pyramidal neuron collaterals projecting to the DG (Scharfman, 2007), $SERT^{Cre}$-dependent GFP-expressing axons innervate the DG inner-molecular layer in both the hemispheres (Fig. 1E). Therefore, during a specific developmental time window, SERT is transiently expressed in a subset of CA3 pyramidal neurons projecting to CA3, CA1 and DG intrinsic circuits.

Pyramidal neuron-specific SERT knockout ($SERT^{Pyramid\Delta}$) mice

To ablate SERT expression in CA3 pyramidal neurons, we crossed Cre recombinase gene driven by the *Emx1* promoter (Gorski et al., 2002) into $SERT^{fl/fl}$ mice (Chen et al., 2015) to generate $SERT^{fl/fl}$; $Emx1^{Cre/+}$($SERT^{Pyramid\Delta}$) and control $SERT^{fl/fl}$ littermates. In $SERT^{fl/fl}$ littermates, SERT was expressed in subsets of CA3 and mPFC pyramidal neurons and thalamocortical projection neurons from E17 to P10 and in raphe serotonergic neurons throughout life, as expected (Fig. 2A; Fig. S1) (Chen et al., 2015; Lebrand et al., 1998; Soiza-Reilly et al., 2019). $SERT^{Pyramid\Delta}$ abolished SERT mRNA in CA3 and mPFC, while SERT mRNA in the thalamus and raphe nuclei preserved (Fig. 2A).

We confirmed $SERT^{Pyramid\Delta}$ effects on SERT function by 5-HT immunostaining of brain sections from P6 $SERT^{Pyramid\Delta}$ mice and $SERT^{fl/fl}$ littermates. $SERT^{fl/fl}$ mice showed 5-HT immunoreactivity in subsets of CA3 and mPFC pyramidal neurons, in thalamocortical projection neurons as well as in raphe serotonergic neurons, indicating efficient 5-HT uptake by these glutamatergic neurons (Fig. 2B) (Chen et al., 2015). Consistent with imported 5-HT being effectively degraded in the glutamatergic neurons, 5-HT immunoreactivity in the glutamatergic neurons in $SERT^{fl/fl}$ mice

Development (2022) 149, dev200549. doi:10.1242/dev.200549

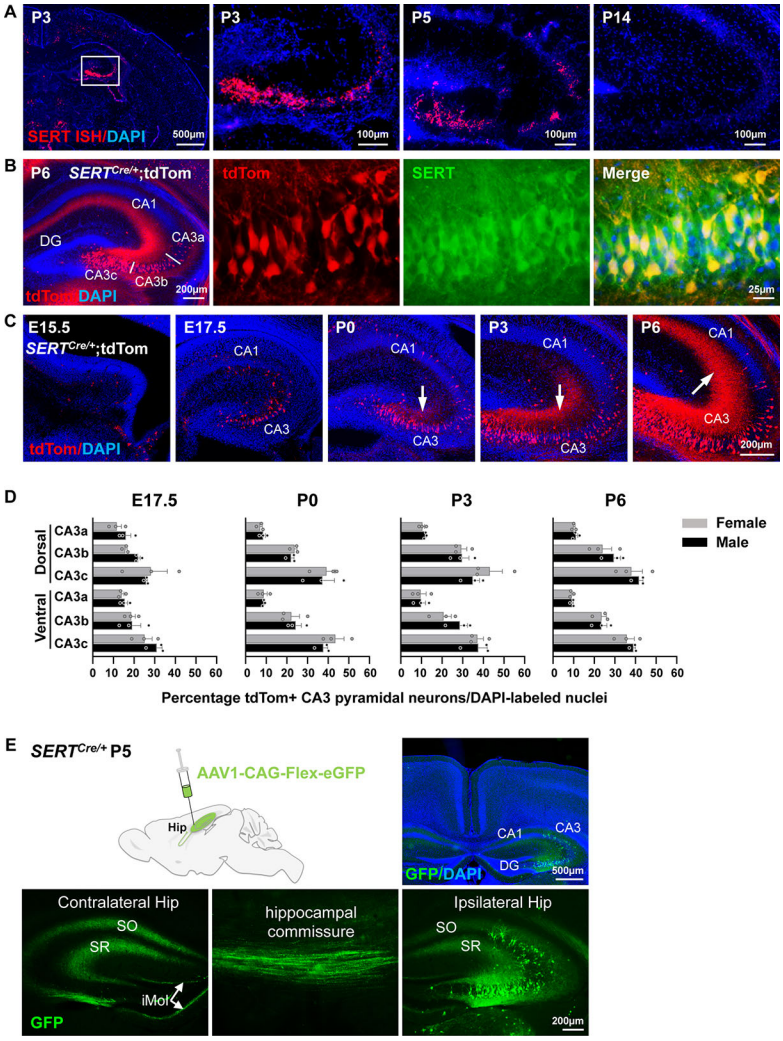

Fig. 1. SERT is specifically expressed in a subset of CA3 pyramidal neurons during hippocampal circuit establishment. (A) Time course of transient SERT expression in CA3. *In situ* hybridization of SERT mRNA on coronal sections of the hippocampus from control mice at indicated ages. The white square indicates the CA3 area shown in the adjacent image at a higher magnification. *n*=3 mice/age. (B) Representative images showing immunolabeled SERT protein in Cre-dependent tdTom-expressing neurons in the hippocampus of P6 $SERT^{Cre/+}$ mice. CA3a, CA3b and CA3c subfields are indicated in the low-magnification image on the left. *n*=7 mice. (C) Representative images showing $SERT^{Cre/+}$-dependent tdTom-expressing neurons arising at E17.5, progressively increasing in number and extending axonal projections (indicated by arrows) in the hippocampus during the first postnatal week. *n*=3 mice/age. (D) Percentage of tdTom-expressing neurons to DAPI-labeled cell nuclei in CA3a, CA3b and CA3c subfields. *n*=3 mice/sex/age. Data are mean±s.e.m., two-way ANOVA followed by Turkey and Šidák post-hoc tests (Table S1). (E) SERT-expressing CA3 pyramidal neuron axonal projection network revealed by AAV-mediated anterograde tracing. Top left, a schematic of unilateral stereotaxic injection of the AAV1.CAG.Flex.eGFP.WPRE.bGH virus into the hippocampus of P5 $SERT^{Cre/+}$ pups. Top right, GFP^+ neurons at the injection site at P18. Bottom, representative images showing GFP^+ axonal projections to the stratum oriens (SO), stratum radiatum (SR) and DG inner-molecular layer (iMol) both at the ipsilateral-hippocampus and via the commissural pathway to the contralateral hippocampus. Six replicates, two females and four males.

was observed only when the pups were treated with the MAOA inhibitor clorgyline, contrasting with robust raphe neuron 5-HT immunoreactivity with or without clorgyline treatment. In $SERT^{PyramidΔ}$ pups, clorgyline treatment conferred 5-HT immunoreactivity in those thalamic neurons but not in CA3 and mPFC pyramidal neurons, while 5-HT immunoreactivity in the raphe neurons was observed with or without clorgyline treatment (Fig. 2B). These observations are in line with previous findings in rodents and *C. elegans* that SERT-expressing glutamatergic terminals function as a local '5-HT degradation sink', absorbing extracellular 5-HT then degrading it to prevent excessive trophic 5-HT signaling (Chen et al., 2015; Jafari et al., 2011).

Because $SERT^{PyramidΔ}$ also ablates SERT expression in the mPFC pyramidal neurons, to exclude a cortical SERT origin in hippocampus development we confirmed a lack of SERT-expressing mPFC pyramidal neuron innervation to the hippocampus, through virus-mediated whole-brain anterograde tracing of SERT-expressing mPFC neurons in $SERT^{Cre/+}$ mice. Consistent with previous observations (Soiza-Reilly et al., 2019), we observed in both male and female mice mPFC SERT-expressing neuron innervation of a wide range of cortical and subcortical regions but not of the hippocampus (Fig. S4, *n*=3 mice/sex). We therefore investigated $SERT^{PyramidΔ}$ effects on hippocampal synaptic circuit development and its long-lasting impacts on adult hippocampal circuitry.

$SERT^{PyramidΔ}$ impairs postnatal synaptic developmental trajectory of the hippocampus

The timing of SERT expression in the CA3 pyramidal neurons coincides with functional circuit establishment in the hippocampus. Although the gross hippocampal structure in mice is formed by birth, functional synaptic circuits between CA3, CA1 and DG develop during the first two postnatal weeks (Leinekugel, 2003). About 85% of adult DG granule cells arrive in the hippocampus between P3 and P10 (Altman and Das, 1966; Bayer, 1980). Likewise, a significant proportion of prenatally born pyramidal neuron precursors attain the pyramidal layer after a developmental sojourn, growing axons and dendrites during this period to assemble into functional circuits (Altman and Bayer, 1990). One attractive scenario is that SERT expression in the CA3 pyramidal neuron terminals shapes hippocampal circuits, in part, by regulating synaptic patterning during the circuit assembly. We tested this idea by examining postnatal development of neurons expressing GFP driven by a *Thy1* promoter cassette, *Thy1-GFP/M* (Feng et al., 2000), in $SERT^{PyramidΔ}$ mice versus control littermates.

Transgenes driven by distinct *Thy1* promoter elements each confer stable reporter expression restricted to subgroups of neurons with shared distinct neurogenesis and synaptogenesis time windows, allowing visualization and tracking of the development of the same neuronal populations in a defined brain region (Deguchi et al., 2011; Feng et al., 2000). Among the *Thy1-GFP* transgenic lines

Development (2022) 149, dev200549. doi:10.1242/dev.200549

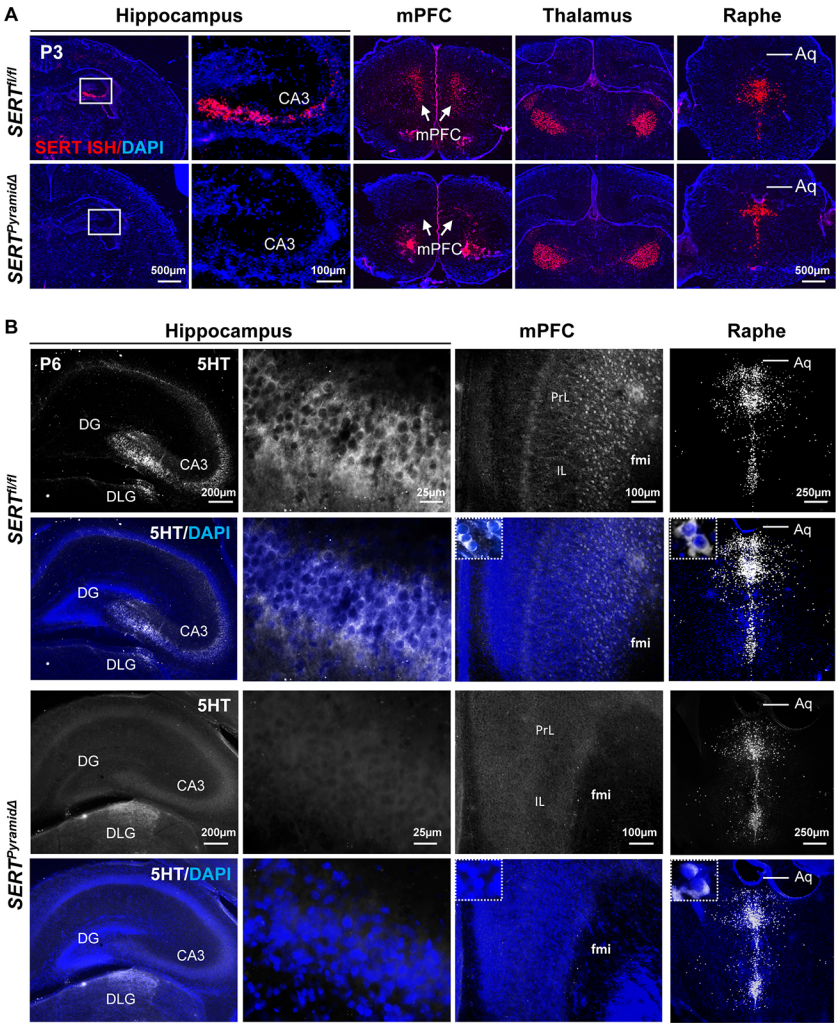

Fig. 2. Conditional SERT knockout in pyramidal neurons (*SERT*^{PyramidΔ}). (A) Representative images of *in situ* hybridization of SERT mRNA on coronal brain sections from *SERT*^{PyramidΔ} mice and *SERT*$^{fl/fl}$ littermates at P3. White squares indicate the CA3 area shown in corresponding adjacent images at higher magnification. *SERT*^{PyramidΔ} abolished SERT expression in CA3 and mPFC, but not in the thalamus and raphe nuclei. *n*=4 mice/genotype. (B) Representative images of 5-HT immunostaining of coronal brain sections of *SERT*^{PyramidΔ} and *SERT*$^{fl/fl}$ littermate mice age P6. Insets show 5-HT immunostaining and DAPI overlay at a higher magnification. In *SERT*^{PyramidΔ} mice, 5-HT immunoreactivity in CA3 and mPFC, but not in thalamic and raphe, neurons was dramatically diminished. Images are representative of three independent experiments, each with two mice/genotype. DLG, dorsal geniculate nucleus; PrL, prelimbic cortex; IL, infralimbic cortex; fmi, forceps minor; Aq, aqueduct.

generated by Feng et al. (2000), the *Thy1-GFP/M* transgene is selectively expressed in subpopulations of postnatally developing pyramidal neurons and DG granule cells (Fig. 3A). The GFP$^+$ cells emerged at the pyramidal layer and DG at P3, progressively increasing in number, growing characteristic dendritic trees and reached adult levels around P16 (Fig. 3A). At P6, 12.2±0.71% and 24.9±2.51% of GFP$^+$ CA1 and DG neurons, respectively, expressed immature neuronal marker Sox2, and only 16.8±5.25% of GFP$^+$ CA1 pyramidal neurons displayed 3rd order apical dendritic branches (Fig. S5). At P16, Sox2 expression was extinguished in nearly all GFP$^+$ CA1 pyramidal neurons, and 93.0±4.55% of GFP$^+$ CA1 pyramidal neurons displayed 3rd and higher order apical dendritic branches (Fig. S5). As CA1 is the major target of CA3 pyramidal neuron Schaffer collaterals, we used *Thy1-GFP/M*-expressing CA1 pyramidal neurons as a model to examine postnatal dendritic development in a target region of SERT-expressing CA3 pyramidal neurons.

We observed a similar timing of GFP$^+$ neuron emergence in *SERT*^{PyramidΔ} versus control mice, and quantitating GFP$^+$ neurons in the entire CA1 region in serial sections across the hippocampus showed a non-significant trend towards a reduction in the total number of GFP$^+$ CA1 pyramidal neurons in *SERT*^{PyramidΔ} mice (Fig. 3B). Three-dimensional reconstruction analyses of GFP$^+$ CA1 pyramidal neuron apical dendritic trees from P16 mice showed no difference between the two genotypes in terms of the branch number and total dendrite length of the entire dendritic trees or 3rd order branches located at the stratum radiatum – the CA3 Schaffer collateral innervation field (Fig. 3C). In contrast, spine morphometric analyses of 3rd order GFP$^+$ dendritic branches showed significantly reduced densities of spines, particularly thin type (immature) spines, in *SERT*^{PyramidΔ} mice (Fig. 3D-F). These observations suggest that CA3 SERT function is essential for normal dendritic spine development of those late-developing CA1 pyramidal neurons, but is not required for the neurons to attain CA1 and their general dendrite growth.

We then asked how disrupting this transient CA3 SERT expression in the development may affect dendritic spine architecture of the adult hippocampus. Dendritic spine architecture reflects a dynamic process driven by correlated neural activity resulting in strengthening or pruning of synapses (Berry and Nedivi, 2017). Reduced immature dendritic spines observed in P16 *SERT*^{PyramidΔ} mice could reflect a temporal delay in synapse formation that may be overcome in the adult hippocampus. Alternatively, this may result in a life-long reduction in synaptic connectivity. We characterized spines on 3rd order branches of *Thy1-GFP/M*-expressing CA1 pyramidal neurons in the same area in 12±2 weeks old *SERT*^{PyramidΔ} mice and control littermates. We observed no difference in thin spine densities between the two genotype groups, and, furthermore, the density of mushroom-shape (mature) spines was significantly increased in *SERT*^{PyramidΔ} mice (Fig. 3G,H). Together, these data suggest that CA3 SERT regulates target region dendritic spine development during circuit assembly,

Development (2022) 149, dev200549. doi:10.1242/dev.200549

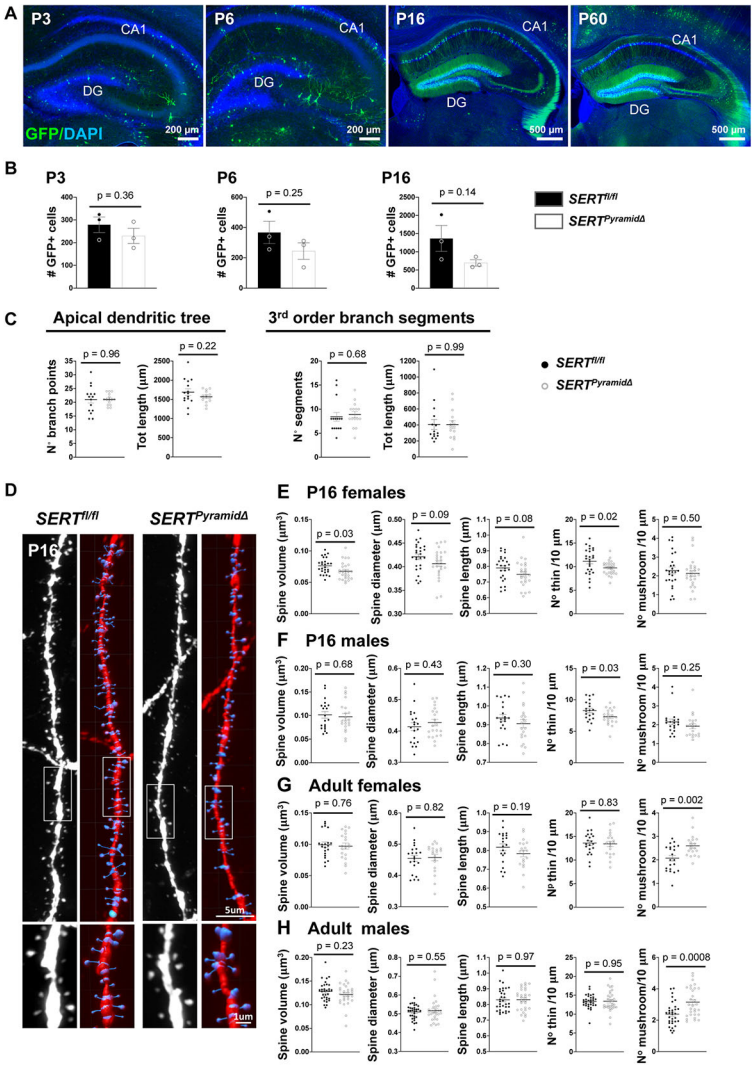

Fig. 3. *SERT*^{PyramidΔ} impairs postnatal development of CA1 pyramidal neuron dendritic spines, secondarily resulting in increased mushroom type mature spine density on adult CA1 pyramidal neurons. (A,B) *Thy1-GFP*/*M*-expressing neurons develop postnatally in the hippocampus. (A) Representative images of *Thy1-GFP*/*M*-expressing neurons in hippocampal coronal sections from *SERT*$^{fl/fl}$ mice at various postnatal stages. (B) Number of GFP^{+} neurons in the CA1 pyramidal layer in serial coronal sections throughout the hippocampus in *SERT*^{PyramidΔ} mice and *SERT*$^{fl/fl}$ littermates at indicated ages. *n*=3 mice/age/genotype. Data are mean±s.e.m. two-tailed *t*-test. (C) 3D dendritic tree reconstruction analyses of *Thy1-GFP*/*M*-expressing CA1 pyramidal neurons showed no difference in the number of branching points or the total length of the dendrites of the entire apical dendritic trees and 3rd order branch segments in *SERT*^{PyramidΔ} mice versus *SERT*$^{fl/fl}$ littermates age P16. Fifteen neurons from three *SERT*$^{fl/fl}$ mice and 15 neurons from three *SERT*^{PyramidΔ} mice. Data are mean±s.e.m, two-tailed *t*-test. (D) Representative images of 3rd order apical dendritic segments of *Thy1-GFP*/*M*-expressing CA1 pyramidal neurons in *SERT*^{PyramidΔ} mice and *SERT*$^{fl/fl}$ littermates age P16. Dendritic segments in collapsed *z*-stack confocal images (white) and corresponding 3D rendering of the segments (red) were subjected to semi-automatic spine morphometric analyses using Imaris. Areas outlined by white boxes are shown at a higher magnification in the bottom panels. (E,F) Spine morphometric analyses of 50 µm long, 3rd order *Thy1-GFP*/*M*-expressing apical dendritic segments located in the stratum radiatum in *SERT*^{PyramidΔ} mice and *SERT*$^{fl/fl}$ littermates age P16. Females, 26 segments from three mice/genotype; males, 21 segments for *SERT*^{PyramidΔ} and 20 segments for *SERT*$^{fl/fl}$ from four mice/genotype. Data are mean±s.e.m. two-tailed *t*-test. (G,H) Spine morphometric analyses of 50 µm long, 3rd order *Thy1-GFP*/*M*-expressing apical dendritic segments located in the stratum radiatum in *SERT*^{PyramidΔ} mice and *SERT*$^{fl/fl}$ littermates age 12±2 weeks old. Females, 20 segments from four *SERT*^{PyramidΔ} mice and 21 segments from three *SERT*$^{fl/fl}$ littermates. Males, 30 segments from five *SERT*^{PyramidΔ} mice and 32 segments from four *SERT*$^{fl/fl}$ littermates. Data are mean±s.e.m. two-tailed *t*-test.

and impaired initial spine development resulted in a secondary long-lasting compensatory increase in mature mushroom spines in the adult hippocampal circuits.

Perinatal SERT expression in pyramidal neurons is required for development of normal activity-dependent hippocampal synaptic plasticity

We next asked whether the transient developmental CA3 SERT expression is essential for normal adult hippocampal synaptic function, by examining presynaptic transmission and long-term, activity-dependent synaptic plasticity at CA3 Schaffer collaterals to CA1 synapses in hippocampal slices from 7- to 8-week-old *SERT*^{PyramidΔ} mice and control littermates. We first confirmed that SERT is not required for general cell fate specification of SERT-expressing CA3 pyramidal neurons (Fig. S3D). We next evaluated basal presynaptic function with paired-pulse stimulus response profiles, using pairs of stimuli at 10-500 ms intervals. We observed no difference in paired-pulse responses at any interval tested between the two genotypes (Fig. 4A), suggesting no significant alterations in presynaptic release probability at Schaffer collateral terminals of *SERT*^{PyramidΔ} mice using this measure.

We then evaluated stimulus-evoked long-term potentiation (LTP) and long-term depression (LTD) of synaptic strength at the Schaffer collateral-CA1 synapses. We observed no significant difference in high-frequency theta bust induced LTP of *SERT*^{PyramidΔ} versus control male mice (Fig. 4B). In marked contrast, the magnitude of LTP was significantly elevated in female *SERT*^{PyramidΔ} mice compared with control females (Fig. 4B).

Contrary to a female-specific *SERT*^{PyramidΔ} effect on LTP, the magnitude of LTD elicited by low frequency Schaffer collateral stimulation was significantly diminished in both male and female *SERT*^{PyramidΔ} mice versus sex-matched littermate controls (Fig. 4C). These results indicate that CA3 SERT is essential for normal development of long-term activity-dependent synaptic plasticity in the hippocampus, and that disruption of this early SERT function results in shared changes in both males and females and sex-biased changes in CA3-CA1 synaptic plasticity. Considering the normal paired-pulse responses, those changes observed in *SERT*^{PyramidΔ} mice involve, at least in part, altered activity-dependent postsynaptic mechanisms.

Disruption of perinatal SERT expression in pyramidal neurons leads to sex-biased behavioral impairments

Early life SSRI exposures have been linked to altered brain activities in infants and to neuropsychiatric disorders including ASD, but some studies failed to detect a statistical significance (Lugo-Candelas et al., 2018; Malm et al., 2016; Olivier et al., 2013). In rodents, SSRI treatments from P3 to P21 result in elevated despair in forced swimming test (FST), and reduced exploratory behaviors in elevated plus maze (EPM) and open field (Ansorge et al., 2004;

Development (2022) 149, dev200549. doi:10.1242/dev.200549

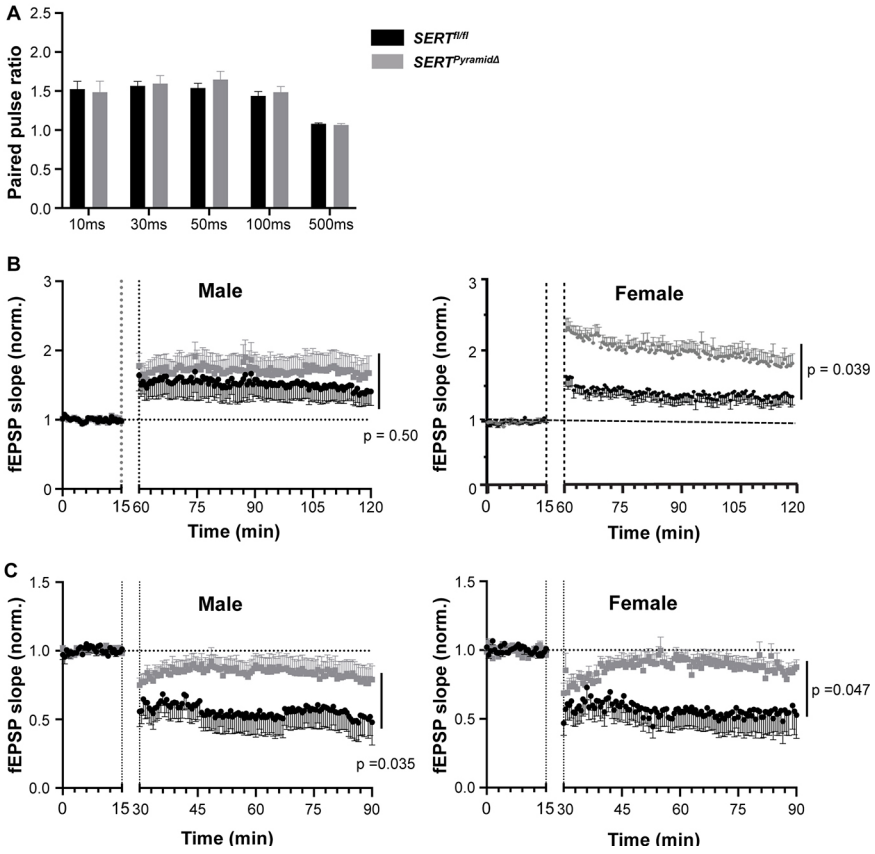

Fig. 4. *SERT*$^{Pyramid\Delta}$ leads to long-term activity-dependent hippocampal synaptic plasticity impairments. (A) Paired-pulse facilitation profiles (PPFs) at Schaffer collateral-CA1 synapses in hippocampal slices, measured at inter-stimulus intervals from 10 to 500 ms. *SERT*$^{fl/fl}$, eight slices from four male and 13 slices from four female mice. *SERT*$^{Pyramid\Delta}$, 12 slices from four male and 11 slices from four female mice. Data are mean±s.e.m. P>0.90, two-way ANOVA for repeated measures. (B) Time course and magnitude of LTP evoked by high frequency theta burst Shaffer collateral stimulation. Males, 11 slices from five *SERT*$^{Pyramid\Delta}$ mice and eight slices from four *SERT*$^{fl/fl}$ littermates. Females, 11 slices from seven *SERT*$^{Pyramid\Delta}$ mice and 11 slices from five *SERT*$^{fl/fl}$ littermates. Each point is normalized to the averaged baseline and data are mean±s.e.m., two-tailed *t*-test. (C) Time course and magnitude of LTD elicited by low frequency Schaffer collateral stimulation. Males, 16 slices from seven *SERT*$^{Pyramid\Delta}$ mice and eight slices from four *SERT*$^{fl/fl}$ littermates. Females, seven slices from four *SERT*$^{Pyramid\Delta}$ mice and nine slices from five *SERT*$^{fl/fl}$ littermates. Each point is normalized to the averaged baseline and data are mean±s.e.m. two-tailed *t*-test.

Glover and Clinton, 2016). Our observations of altered CA3-CA1 synaptic plasticity in *SERT*$^{Pyramid\Delta}$ mice prompted us to test whether disrupting the temporal-specific SERT expression in the pyramidal neurons during the circuit assembly could be a cause for certain altered behaviors. We observed sex-biased behavioral deficits in *SERT*$^{Pyramid\Delta}$ mice versus sex-matched controls. Male, not female, *SERT*$^{Pyramid\Delta}$ mice displayed increased immobility time in FST (Fig. 5A). Likewise, in the EPM, male but not female *SERT*$^{Pyramid\Delta}$ mice spent significantly less time and traveled less distance in open arms, although total distances traveled during the assay period were comparable between the two genotype groups (Fig. 5B). In the open field, the total time spent in a defined central area was comparable between the two genotypes; however, *SERT*$^{Pyramid\Delta}$ females displayed a significant tendency to avoid traveling to the center of the open field, as measured by increased mean distance from the center point of the open field (Fig. 5C).

We further assessed *SERT*$^{Pyramid\Delta}$ effects on social behaviors, a measure frequently used for ASD-related behavioral phenotypes in mouse models (Auerbach et al., 2011; Platt et al., 2017; Tang et al., 2014). The test measures social interactions of test mice with an unfamiliar mouse versus an empty cup, and then measures social novelty by replacing the empty cup with a novel unfamiliar mouse (Fig. 5D,E). We measured the social interactions in two-time bins of 4.5 min each. During the first-time bin, *SERT*$^{Pyramid\Delta}$ and control mice all displayed a preference for the mouse over the empty cup. In the second-time bin, however, although control mice continued to display a significant preference for the mouse, both male and female *SERT*$^{Pyramid\Delta}$ mice showed no significant preference for the mouse versus the empty cup (Fig. 5D). In the social novelty test, control but neither male nor female *SERT*$^{Pyramid\Delta}$ mice showed a significant preference for the novel mouse (Fig. 5E).

Contextual memory of fear conditioning has been applied to measure hippocampal functional integrity (Kim and Fanselow, 1992; Phillips and LeDoux, 1992). During the contextual fear conditioning with three consecutive electrical shocks, we observed no genotype effect on the immediate response to the shocks (Fig. 5F). The contextual memory was measured daily for the subsequent 10 days, based on freezing time when mice were placed into the test apparatus with the identical context. *SERT*$^{Pyramid\Delta}$ females displayed significantly reduced freezing time compared with control females. In contrast, we observed no difference in freezing behavior of male *SERT*$^{Pyramid\Delta}$ versus control male mice (Fig. 5F).

To more granularly assess the *SERT*$^{Pyramid\Delta}$ effects on males versus females, we further analyzed the behavioral datasets using two-way ANOVA followed by Šidák's multiple comparison test (Table S1). There was a significant genotype effect over FST ($F_{1,67}$=5.29, P=0.0245) and EPM (open arm time: $F_{1,48}$=4.29, P=0.0438), with a significant (FST, P=0.0373 vs P=0.6189) and a strong trend (EPM, P=0.0717 vs P=0.7055) of deficits only in male *SERT*$^{Pyramid\Delta}$ mice. There was a strong trend for the genotype X sex interaction effects on avoiding the center point of the open field ($F_{1,48}$=3.82, P=0.0566) with a significant deficit only in the females (P=0.0466). In order to perform two-way ANOVA for social behaviors, we calculated the social interaction index and social novelty index for each mouse (Walsh et al., 2018) and observed no genotype or sex effect according to these measures (Table S1).

These data suggest that disruption of the transient pyramidal neuron SERT expression during development may lead to a range of cognitive behavioral deficits. Statistical analyses imply that SERT may regulate the development of neural circuits underlying these behaviors in both males and females, but specific behavioral

Development (2022) 149, dev200549. doi:10.1242/dev.200549

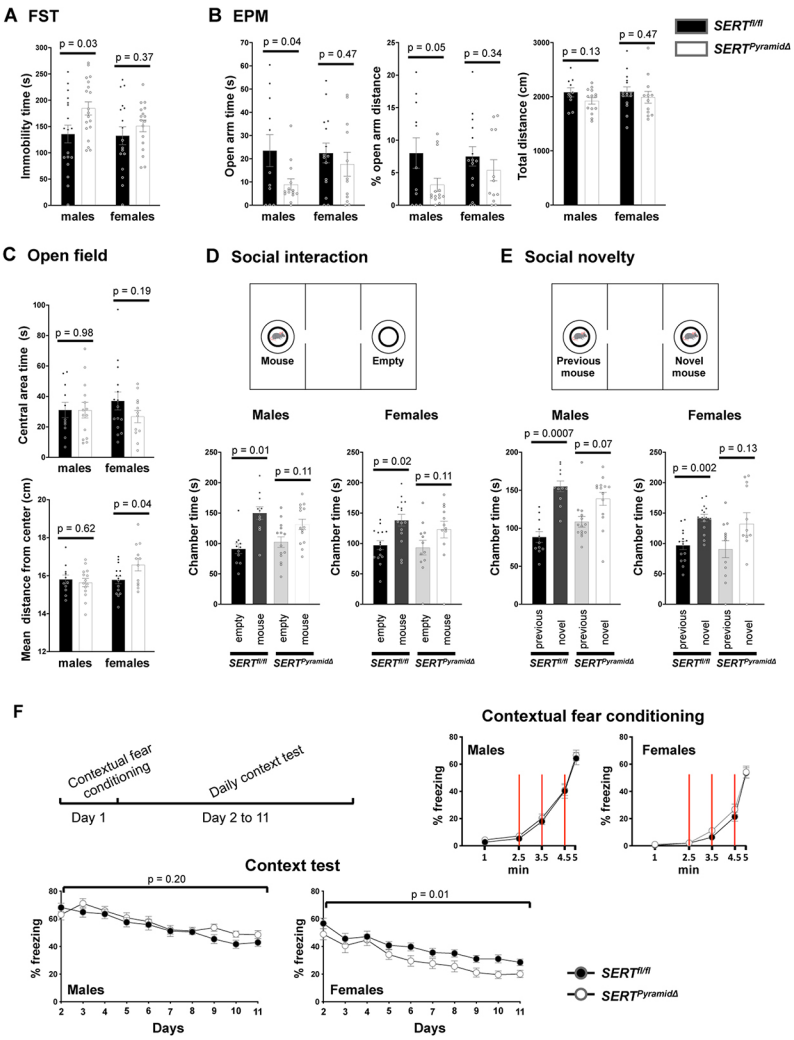

Fig. 5. Sex-biased behavioral changes in adult *SERT*$^{Pyramid\Delta}$ mice. (A) FST. Male, but not female, *SERT*$^{Pyramid\Delta}$ mice showed increased immobility time versus sex-matched control mice. Eighteen *SERT*$^{fl/fl}$ and 19 *SERT*$^{Pyramid\Delta}$ males, 17 *SERT*$^{fl/fl}$ and 17 *SERT*$^{Pyramid\Delta}$ females. Data are mean±s.e.m. two-tailed *t*-test. (B) EPM test. Male, but not female, *SERT*$^{Pyramid\Delta}$ mice spent less time and traveled less distance in the open arms versus sex-matched control mice. Data are mean±s.e.m., two-tailed *t*-test. (C) Open field test. Top panel, *SERT*$^{Pyramid\Delta}$ and sex-matched control mice spent comparable time in the central square area. Bottom panel, mean distance from the center point of the open field was increased for *SERT*$^{Pyramid\Delta}$ females. Data are mean±s.e.m., two-tailed *t*-test. (D) Three-chambered social interaction test. Both male and female *SERT*$^{Pyramid\Delta}$ mice displayed no significant preference for a mouse versus an empty cup. Data are mean±s.e.m. paired two-tailed *t*-test. (E) Three-chambered social novelty test. Both male and female *SERT*$^{Pyramid\Delta}$ mice displayed no significant preference for a novel mouse versus a familiar mouse. Data are mean±s.e.m, paired two tailed *t*-test. (F) Contextual fear memory test. Top left, experimental protocol. Top right, freezing responses to shocks (indicated by red lines) in the training session. Bottom, contextual memory measured as the percentage of freezing time in the same context used for the training. Each data point is mean±s.e.m. The performance over the entire testing period was evaluated by a mixed effect model accounting for longitudinal data: Males, P=0.2014, $F_{1,23}$=1.7294; females, P=0.0128, $F_{1,24}$=7.2305. The same cohort, 11 *SERT*$^{fl/fl}$ and 14 *SERT*$^{Pyramid\Delta}$ males, 15 *SERT*$^{fl/fl}$ and 12 *SERT*$^{Pyramid\Delta}$ females, was tested in assays B to F as detailed in the Materials and Methods. P values are indicated on the top of the bars.

impairments may be more pronounced in males or females relative to sex-matched controls. All the tested behaviors depend on hippocampal and mPFC function, and *SERT*$^{Pyramid\Delta}$ ablates SERT expression in both the CA3 and mPFC pyramidal neurons (Fig. 2). Future studies are needed to elucidate how CA3 and mPFC SERT-expressing pyramidal neuron terminals may coordinate circuit assembly in their respective target brain regions in functionally defined circuits underlying these behaviors in males versus females.

Disruption of SERT expression in pyramidal neurons causes sex-specific transcriptional dysregulation in early postnatal hippocampus

Transcriptomic analyses of brain tissues from ASD and schizophrenia subjects and mouse models suggest that sex-biased pathological phenotypes may derive, in part, from transcriptional dysregulation of different gene sets in males and females (Hoffman et al., 2022; Jung et al., 2018; Werling et al., 2016). To gain insights into the connection between SERT dysfunction during neural circuit assembly and observed *SERT*$^{Pyramid\Delta}$ phenotypes, we carried out RNA-seq analyses to examine the transcriptome of the hippocampus of male and female *SERT*$^{Pyramid\Delta}$ mice versus control littermates age P7. We identified significant transcriptional alterations in *SERT*$^{Pyramid\Delta}$ hippocampus versus sex-matched littermate controls, with little overlap between dysregulated genes in the two sexes (Fig. 6A; Tables S2 and S3).

Consistent with transcriptomes of ASD and schizophrenia subjects (Collado-Torres et al., 2019; Velmeshev et al., 2019; Voineagu et al., 2011), changes in the expression levels in *SERT*$^{Pyramid\Delta}$ versus control hippocampus were generally subtle in magnitude. We identified 42 differentially expressed genes (DEGs) at $P\leq0.005$, 121 DEGs at $P\leq0.01$ and 528 DEGs at $P\leq0.05$ in male *SERT*$^{Pyramid\Delta}$ versus controls, and 46 DEGs at $P\leq0.005$, 131 DEGs at $P\leq0.01$ and 545 DEGs at $P\leq0.05$ in female *SERT*$^{Pyramid\Delta}$ versus controls (Tables S2 and S3).

To assess whether DEGs represent small magnitude but coordinated changes of genes in biological processes and cellular functions, we performed Gene Ontology (GO) analyses of male and female DEGs at $P\leq0.05$ (Fig. 6B; Table S4). Male *SERT*$^{Pyramid\Delta}$ DEGs were preferentially enriched for processes related to transcriptional regulation and neurodevelopment, whereas female *SERT*$^{Pyramid\Delta}$ DEGs enriched for processes related to translation and to a lesser extent to transcription. Male and female *SERT*$^{Pyramid\Delta}$ DEGs both displayed enrichments for synaptic connections and synaptic functions, but in distinct cellular processes and compartments. For example, male DEGs were enriched in ‘synaptic vesicles’ and ‘lamellipodium’, whereas female DEGs were enriched for ‘extracellular exosome’, ‘focal adhesion’ and ‘transmembrane transport’ (Fig. 6B; Table S4). We also identified common GO terms in both *SERT*$^{Pyramid\Delta}$ males and females (e.g. ‘postsynaptic density’, ‘synapses’ and ‘dendritic spines’), yet the DEGs differed between the two sexes (Fig. 6B; Table S4). We further assessed whether

Development (2022) 149, dev200549. doi:10.1242/dev.200549

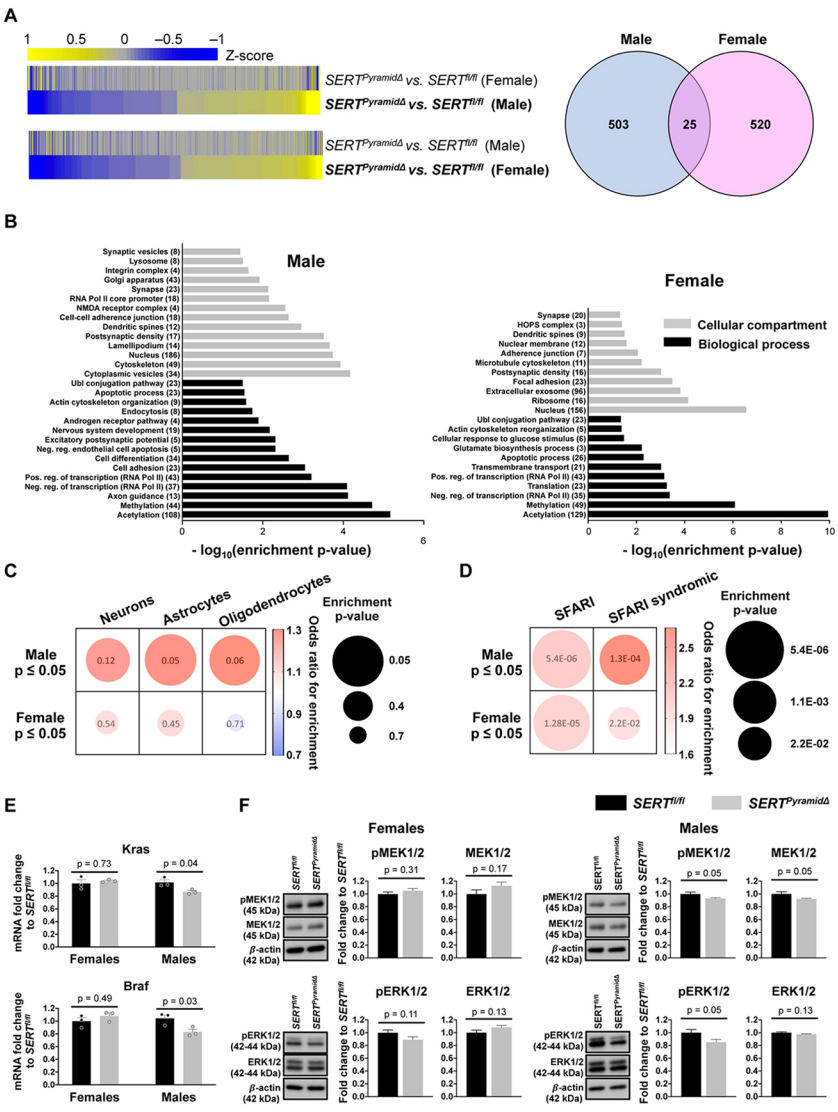

Fig. 6. Sex-biased transcriptional dysregulation in *SERT*^{PyramidΔ} hippocampus age P7. (A) Left, anchored heatmaps comparing *SERT*^{PyramidΔ}-dependent differential gene expression profiles in P7 dorsal hippocampus in the two sexes (DEGs based on $P \leq 0.05$, n=3/group; each n was pooled dorsal hippocampal tissues from four mice, a total of 48 mice for the entire cohort). Normalized RNA expression values (averaged between replicates) were used to generate z-scores for each row. Right, Venn diagram displaying low overlap between DEGs in male and female *SERT*^{PyramidΔ} mice versus sex-matched controls. (B) Gene Ontology for DEGs in P7 male and female *SERT*^{PyramidΔ} dorsal hippocampus. Gray bars indicate GO terms categorized by cellular compartments; black bars indicate GO terms categorized by biological processes. The number of DEGs matching each category is indicated in parentheses. DEGs were based on $P \leq 0.05$. (C,D) Distinct enrichments of male and female *SERT*^{PyramidΔ} hippocampal DEGs for cell type-specific markers (C), and for ASD-associated and ASD-syndromic genes curated by the SFARI database (D). Circle size indicates Fisher's exact test P value for the enrichment, and color indicates the odd ratio for the enrichment. DEGs were based on $P \leq 0.05$. (E) RT-qPCR analyses of Kras and Braf mRNA levels in dorsal hippocampus of P7 male and female *SERT*^{PyramidΔ} versus *SERT*$^{fl/fl}$ mice. n=3/group; each n was pooled dorsal hippocampal tissues from four mice. Data are mean±s.e.m, two-way ANOVA followed by Šidák post-hoc test. Kras sex effect: $F_{1,8}$=4.425, P=0.0685. Kras genotype X sex interaction: $F_{1,8}$=6.349, P=0.0358. Braf sex effect: $F_{1,8}$=4.324, P=0.0712. Braf genotype X sex interaction: $F_{1,8}$=8.677, P=0.0185. (F) Immunoblotting quantification for pMEK1/2, MEK1/2, pERK1/2 and ERK1/2 in P7 dorsal hippocampal tissue from *SERT*^{PyramidΔ} versus sex-matched *SERT*$^{fl/fl}$ mice. n=6 mice/sex/genotype, data are mean±s.e.m. two-tailed t-test.

sex-biased enrichments in the biological processes and cellular compartments are represented in relatively smaller sets of DEGs at P<0.01 or even at P<0.005, and we observed the same patterns of sex-specific transcriptional dysregulation but in fewer GO terms identified in DEGs at P<0.05 (Tables S5-S8). For example, male DEGs were still enriched with 'acetylation' and 'methylation' terms, and female DEGs remained enriched with the 'ribosome' term (Tables S5-S8). Both male and female DEGs at P<0.01 remained enriched in 'UbI conjugation pathway', but specific DEGs remained different between the two sexes. Even DEGs at P<0.005 were functionally related, with female DEGs enriched with GO terms of 'plasma membrane', 'transport/symport' and 'oxidation-reduction processes', and male DEGs enriched with the GO terms of 'cytoplasmic vesicles', 'cytoskeleton regulation' and 'astrocyte development' (Tables S5-S8).

Our previous studies indicated that SERT expression in glutamatergic terminals controls 5-HT levels at target brains to influence cyto- and synaptic-patterning of diverse neuronal types (Chen et al., 2015; De Gregorio et al., 2020). We therefore asked whether SERT preferentially regulates gene expression in specific cell types, by aligning *SERT*^{PyramidΔ} DEGs with lists of markers for neurons, astrocytes and oligodendrocytes (Cahoy et al., 2008). Male DEGs at P<0.05 were significantly enriched for astrocytes markers, with a trend towards enrichments of oligodendrocyte markers (Fig. 6C; Table S9). Male DEGs at P<0.01 showed an enrichment of oligodendrocyte markers (Table S9). Male DEGs at P<0.005 were significantly enriched in the GO term of 'astrocyte development'. By contrast, females DEGs at any P-value threshold displayed no enrichment for any cell type-specific markers (Fig. 6C, Table S9).

Given social interaction behavioral impairments in mouse models of disparate ASD-associated variants, we analyzed the overlap between *SERT*^{PyramidΔ} DEGs and ASD-associated genes curated by the SFARI database. Both male and female DEGs at P<0.05 were significantly enriched for ASD-associated as well as ASD-syndromic genes (Fig. 6D; Table S9). The significance of enrichment of ASD-associated genes was substantially increased with male DEGs at P<0.01 and also at P<0.005, contrasting with no statistically significant enrichments of ASD-associated genes in female DEGs at P<0.01 and P<0.005 (Table S9).

We validated bioinformatic predictions by focusing on the well-established RAS-RAF-MEK-ERK kinase pathway (Fig. 6E,F). Both Kras and Braf were reduced in male *SERT*^{PyramidΔ} transcriptome compared with sex-matched controls (Tables S2 and S3). RT-qPCR confirmed significantly reduced *Kras* and *Braf* expression levels in P7 male but not in female *SERT*^{PyramidΔ} hippocampus (Fig. 6E), whereas SERT mRNA was dramatically

Development (2022) 149, dev200549. doi:10.1242/dev.200549

reduced to the same extend in the male and female samples (Fig. S6). Ingenuity pathway analyses (Qiagen) identified *Kras* and *Braf* in multiple relevant canonical GO pathways in the male DEG set (Tables S10, S11). Kras and Braf regulate neural circuit development and function in part by regulating phosphorylation of MEK and ERK kinases (Albert-Gascó et al., 2020; Eblen, 2018). We therefore examined Kras and Braf activity by western blotting analyses of MEK and ERK phosphorylation levels in P7 male and female $SERT^{PyramidΔ}$ versus control hippocampus. We observed no difference in the levels of MEK and ERK, and their phosphorylated forms in $SERT^{PyramidΔ}$ versus control females (Fig. 6F). In contrast, phosphorylated MEK and ERK levels were significantly attenuated in $SERT^{PyramidΔ}$ males (Fig. 6F). In addition, the total level of MEK protein was also reduced in $SERT^{PyramidΔ}$ males. Taken together, these data indicate that CA3 SERT serves to regulate gene expression during hippocampal circuit assembly, and suggest that sex differences in the synaptic and behavioral impairments of $SERT^{PyramidΔ}$ mice may stem, in part, from aberrant gene expression patterns during the establishment of the neural circuits.

DISCUSSION

This study provides the first characterization of the role of transient SERT expression in non-serotonergic neurons in the development of hippocampus. We unexpectedly found that disruption of SERT expression in CA3 and mPFC pyramidal neurons causes sex-biased gene expression alterations during hippocampal circuit assembly, sex-distinct impairments in long-term activity-dependent synaptic plasticity and a range of cognitive behaviors. Our study revealed that the temporal- and brain region-specific SERT function during synaptic circuit assembly is essential for normal cognitive function and behaviors in males versus females.

Unlike in adult brain, where 5-HT is released at synapses as a neurotransmitter, 5-HT is mainly a trophic factor in developing brain (Azmitia, 1999; Gaspar et al., 2003). Raphe serotonergic neurons release 5-HT throughout the brain before synapses are formed. In addition, 5-HT from peripheral origins may penetrate into the developing brain (Bonnin and Levitt, 2011; Cote et al., 2007). The timing of CA3 SERT expression coincides with the period of activity-dependent metaplasticity in the hippocampus (McHail and Dumas, 2015). Multiple studies have demonstrated global reconfiguration of gene expression patterns during neuronal maturation (Li et al., 2018; Lister et al., 2013; Mo et al., 2015). The transient SERT expression in glutamatergic terminals may couple diverse physiological and environmental cues into regional 5-HT signaling and its downstream gene regulatory mechanisms in functionally related neuronal types and their potential future responses to neuronal activity.

SERT function and a critical period of neural circuit development

Two remarkable aspects of SERT function in the developing hippocampus are: (1) its exclusive expression in CA3 neurons – the relay neurons of hippocampal intrinsic circuits – hence dedicated to local circuit assembly; and (2) its exquisite temporal-specific expression, suggesting that certain aspects of hippocampal cognitive capabilities are shaped by the levels of 5-HT during this time window. Critical periods of synaptic circuit assembly have been studied extensively in primary sensory systems, although critical periods for higher cognitive function establishment are less well understood (Hensch, 2004). It has long been appreciated that subpopulations of embryonically born hippocampal excitatory neurons take a developmental sojourn, completing their differentiation during functional circuit assembly (Altman and Bayer, 1990). In addition, diverse GABAergic neuron subtypes attain hippocampus during this period (Lim et al., 2018; Wamsley and Fishell, 2017). This neuronal population expansion is thought to shape cognitive capabilities and complex behaviors (Lee et al., 2014; Silbereis et al., 2016; Stiles and Jernigan, 2010). Using *Thy1-GFP/M*-expressing CA1 pyramidal neurons as a model, we demonstrated that SERT is essential for normal dendritic spine development of those late-developing neurons but is not required for the ability to attain the terminal brain destination and the gross dendrite growth. These findings are consistent with the notion that regulation of cortical projection neuron identity and maturation processes are mechanistically separable (Cadwell et al., 2019; Rakic et al., 2009). Our data suggest that CA3 SERT is dedicated to modulating neuronal functional maturation processes to elaborate adult hippocampal synaptic circuitry.

We demonstrated in $SERT^{PyramidΔ}$ mice that *Thy1-GFP/M*-expressing CA1 pyramidal neurons display reduced dendritic thin spines at P16 but increased mushroom-shape mature spines in the adulthood. Previous studies have shown that disrupting SERT expression in mPFC pyramidal neurons or SSRI exposure (P2-P14) causes increased functional PFC glutamatergic synapses at their subcortical target regions at 4 weeks of age (Soiza-Reilly et al., 2019). SERT-expressing glutamatergic neurons have been shown to regulate synaptic development of multiple neuronal types, both excitatory and GABAergic neurons, across their target brain regions (Chen et al., 2015; De Gregorio et al., 2020). This suggests that SERT-expressing glutamatergic terminals may coordinately regulate trophic 5-HT signaling to, in turn, modulate synaptic development of disparate neuronal types at the local circuits. Consistent with our finding that 5-HT is quickly degraded in these glutamatergic neurons, previous studies in *C. elegans* and mice demonstrated that SERT-expressing glutamatergic neurons do not exert the function by releasing imported 5-HT, and disrupting SERT function in the glutamatergic neurons results in excessive 5-HT (Chen et al., 2015; Jafari et al., 2011; Persico et al., 2001). We identified a gradient distribution pattern of CA3 SERT-expressing neurons increasing from CA3a towards CA3c throughout dorsoventral hippocampal axis. SERT function may therefore generate a gradient of 5-HT along the target regions specifically during local circuit assembly; disrupting this SERT function impairs the pattern of synaptic development, secondarily resulting in hyperconnectivity in the adult circuits.

Increased dendritic spine densities are a common feature observed in postmortem brains of a variety of neurodevelopmental disorders (Phillips and Pozzo-Miller, 2015). Examining postmortem brains identifies substantially higher dendritic spine densities in adolescence ASD brains, with no significant differences between ASD and typical brains at 2-9 years old (Tang et al., 2014). It is possible that increased spine density observed in several neurodevelopmental diseases reflects a common secondary compensatory response to perturbations of circuit assembly by diverse genetic and environmental insults. Interestingly, ablating the ASD risk gene *Shank3* in mice causes increased synapses during circuit development but hypoconnections in adulthood (Peça et al., 2011; Peixoto et al., 2016). These findings highlight the importance of identifying both the origin of anatomical alterations induced by genetic and environmental insults causing circuit derailment and the end-point differences.

SERT function during circuit assembly and behaviors

Electrophysiological assessments implicate perinatal CA3 SERT in shaping the long-term, activity-dependent synaptic plasticity

Development (2022) 149, dev200549. doi:10.1242/dev.200549

of hippocampal circuits. As mushroom spines are indicative of functional spines (Berry and Nedivi, 2017), it is tempting to think that increased CA1 mushroom spine density diminished CA3-CA1 synaptic plasticity in *SERT*^{PyramidΔ} mice. However, despite shared *Thy1-GFP/M*-expressing CA1 pyramidal neuronal dendritic spine phenotypes, changes in CA3-CA1 long-term synaptic plasticity in male and female *SERT*^{PyramidΔ} mice differed. Both *SERT*^{PyramidΔ} males and females showed diminished LTD at Schaffer collateral-CA1 synapses, but only *SERT*^{PyramidΔ} females displayed larger LTP at these synapses. *Tsc2*$^{+/−}$ and *Fmr1*-KO mice are the two best studied ASD mouse models and both display increased CA1 pyramidal neuron dendritic spine density, yet LTD at Schaffer collateral-CA1 synapses is attenuated in *Tsc2*$^{+/−}$ mice but enhanced in *Fmr1*-KO mice (Auerbach et al., 2011; Dölen et al., 2007; Tang et al., 2014). These observations together support the notion that different, indeed opposite, functional changes may be associated with apparently similar synaptic architectural phenotypes (Mullins et al., 2016).

In line with the sex-biased changes in the hippocampal synaptic plasticity, male and female *SERT*^{PyramidΔ} mice displayed both shared and distinct behavioral impairments. Statistical analyses imply that the development of neural circuits mediating these behaviors are coordinately regulated by SERT, but *SERT*^{PyramidΔ} effects may differ in males versus females (Table S1). All the tested behaviors rely on complex brain circuits, not exclusively regulated by the hippocampus. Indeed, SERT-expressing mPFC pyramidal neurons project to a wide range of cortical and subcortical regions, including amygdala and VTA, the key brain regions for learning and stress responses (Fig. S4) (Soiza-Reilly et al., 2019). Therefore, SERT-expressing pyramidal neuron projection terminals are in the position to coordinate circuit development in the hippocampus, cortex and the subcortical regions to shape sensory perception, cognition and behaviors. Future studies could investigate the molecular mechanisms in each of the brain regions in males versus females regulated by SERT, thus 5-HT, specifically during circuit assembly.

SERT expression in pyramidal neurons and transcription patterning in early postnatal hippocampus

Our transcriptomic analyses shed some light on possible mechanistical roles of SERT expression in the pyramidal neurons. First, SERT may regulate neural circuit assembly, in part, via transcriptional regulation of regional gene expression patterns during this developmental stage. The modest magnitude of multiple DEGs in given GO categories suggests that SERT function may coordinately modulate functional-related components to fine-tune these biological processes.

Second, sex-biased DEGs in postsynaptic density and dendritic spine GO terms suggest that CA3 SERT controls gene expression in neurons at target regions in both males and females, but in distinct molecular mechanisms. In light of the similar dendritic spine and LTD phenotypes observed in male and female *SERT*^{PyramidΔ} CA1, SERT may regulate different genes in CA1 pyramidal neurons in the two sexes. However, as SERT-expressing glutamatergic neurons may regulate multiple cell types at the target regions (Chen et al., 2015; De Gregorio et al., 2020), some sex-biased *SERT*^{PyramidΔ} phenotypes may result from transcriptional dysregulation in different cell types in males versus female hippocampus.

The mechanisms by which SERT regulates gene expression are not known. The 14 5-HT receptor subtypes are expressed in the hippocampus on different cell types (Berumen et al., 2012; Wirth et al., 2017). Interestingly, RNA-seq revealed and RT-qPCR confirmed significantly higher expression levels of Htr1b in both control and *SERT*^{PyramidΔ} females compared with males in P7 hippocampus (Fig. S6). In addition, Htr2c showed a trend towards higher expression in control females versus control males that became significantly higher compared with *SERT*^{PyramidΔ} males (Fig. S6). In contrast, CA3 SERT expression levels were comparable between the two sexes (Fig. S6). Therefore, CA3 SERT may influence hippocampal circuit development via inherent sex-biased expression of 5-HT receptor subtypes. Another intriguing possibility is that trophic 5-HT may directly influence transcription, by covalently attaching to the histone H3 protein at glutamine 5 (H3Q5ser; histone H3 serotonylation) of chromatin (Farrelly et al., 2019; Zhao et al., 2021). Indeed, trophic 5-HT may readily enter diverse cell types, diffuse between the cytoplasm and nucleus, and interact with ‘intracellular targets’ (Buznikov et al., 2001; Colgan et al., 2009). Gennady Buznikov and Jean Lauder have long proposed that 5-HT is an ancient morphogen controlling spatial-temporal organization of ontogenesis before existence of synapse – so-called a ‘prenervous’ neurotransmitter (Buznikov et al., 2001). The brain may have adopted an evolutionary conserved ontogenetic mechanism and expanded it to couple physiological and environmental variations into gene expression patterns, synaptic configuration and circuits.

In human, multiple ASD risk genes, including Chd8 that regulates sex-dimorphic gene expression, are selectively co-enriched in PFC pyramidal neurons in midfetal gestation (Voineagu et al., 2011; Willsey et al., 2013), coinciding with the timing of SERT expression in cortical glutamatergic neurons (Nowakowski et al., 2017). We identified ASD risk genes enriched in DEGs in P7 *SERT*^{PyramidΔ} hippocampus, suggesting that SERT function and these ASD risk genes might intersect during circuit assembly. Notably, a common feature shared between transcriptomes of brain tissues from ASD subjects (Werling et al., 2016) and P7 *SERT*^{PyramidΔ} hippocampus is male-biased enrichments of DEGs in glial cells, particularly astrocytes. The essential, transient SERT function may be one explanation for the difficulty in efforts to ‘reverse’ aberrant neural circuits as a treatment for core disease phenotypes. The phenotypes of *SERT*^{PyramidΔ} mice provide testable paradigms for elucidation of the molecular mechanisms that are crucial for normal neural circuit maturation, may be impaired by some relevant ASD risk genes, and might be genetically and pharmacologically manipulated during this developmental time window for testing the possibility of correcting and/or preventing cognitive and behavioral deficits.

MATERIALS AND METHODS

Mice

Animal use and procedures were approved by the institutional animal care and use committee at the Albert Einstein College of Medicine and New York Medical College. Generation of *SERT*$^{fl/fl}$ mice has been previously described (Chen et al., 2015). *SERT*^{PyramidΔ} mice were generated by crossing *SERT*$^{fl/fl}$; *Emx1-Cre* (Jackson Laboratories 00562) (Gorski et al., 2002) females and *SERT*$^{fl/fl}$ males. Other mouse lines used for this work were: *Thy1-GFP/M* mice (Jackson Laboratories 007788) (Feng et al., 2000), SERT-CRE mice (Jackson Laboratories 014554) (Zhuang et al., 2005) and Ai14 Cre-dependent-tdTomato line (Jackson Laboratories 007914) (Madisen et al., 2010). All the mouse lines were backcrossed to wild-type C57BL/6 for 10-12 generations.

Immunohistochemistry

Mice were anesthetized by intraperitoneal injection of avertin (400 mg/kg) before transcardial perfusion with phosphate-buffered saline (PBS) followed by 4% paraformaldehyde (PFA) in PBS, and brains were dissected. Pups younger than P6 were cryoanesthetized on ice before

Development (2022) 149, dev200549. doi:10.1242/dev.200549

transcardial perfusion. To analyze staged embryonic brains, the conception day was determined based on vaginal plug marks. The day of the vaginal plug mark observed was taken as E0.5. Pregnant mothers were deeply anesthetized using isoflurane, the embryos were removed and embryonic brains collected. Brains were post-fixed overnight in 4% PFA, 75 µm (unless stated otherwise) coronal sections were cut on a vibratome (Leica) and processed immediately for immunostaining. Sections were washed three times for 10 min in PBS, once for 30 min in PBS with 0.3% Triton X-100, and blocked with 5% donkey or goat serum and 0.1% Triton X-100 in PBS for 1 h at room temperature, before incubation with primary antibodies overnight at 4°C in the blocking solution. For BrdU staining, sections were incubated in 2 N HCl for 1 h at room temperature and rinsed three times for 5 min in PBS before applying the blocking solution. For 5-HT staining, $SERT^{PyramidΔ}$ pups and control littermates were injected intraperitoneally with the MAOA inhibitor clorgyline (20 mg/kg, Sigma M3778) or saline 18 h and 3 h before perfusion and Triton X-100 was excluded from all solutions. The following primary antibodies and dilutions were used: rabbit anti-5-HT (1:200, W. M. Steinbusch, University of Limburg, The Netherlands; Sze et al., 2000), rat anti-BrdU (1:500, Abcam, AB6326), rat anti-Ctip2 (1:500, Abcam, AB18465), chicken anti-GFP (1:1000, Abcam, AB13970), rabbit anti-Hub (1:100, Proteintech, 14008-1-AP), goat anti-Prox1 (1:1000, R&D, AF2727-SP), guinea pig anti-SERT (1:500, Frontier Institute, HTT-GP-Af1400), goat anti-Sox2 (1:400, R&D, AF2018) and goat anti-tdTomato (1:500, Sicgen, AB8181-200). Immunostaining of the proteins, BrdU and 5-HT was visualized using secondary antibodies conjugated with fluorescent dye 488, 555, 568 or 647 at a dilution of 1:400. Donkey anti-chicken 488 was purchased from Sigma (SAB460003); and the other secondary antibodies were from Invitrogen [donkey anti-goat 488 (A11055), donkey anti-goat 555 (A21432), donkey anti-mouse 488 (A21202), donkey anti-mouse 555 (A31570), donkey anti-mouse 647 (A31571), donkey anti-rabbit 488 (A21206), donkey anti-rabbit 555 (A31572), donkey anti-rabbit 647 (A31573), donkey anti-rat 488 (A21208), goat anti-guinea pig 488 (A11073), goat anti-guinea pig 555 (A21435), goat anti-guinea pig 647 (A21450), goat anti-mouse 488 (A11029), goat anti-rabbit 488 (A11008), goat anti-rabbit 568 (A11011) and rabbit anti-mouse 568 (A11061)]. Sections were counterstained with DAPI (Thermo Fisher, D1306) to detect cell nuclei. Wide-field microscopy fluorescence images were captured using an Axiocam MR digital camera attached to a Zeiss AxioImager Z1 microscope. Confocal images were acquired using a laser point-scanning Zeiss LSM 880 Airyscan microscope.

Cell counts

Serial coronal sections (75 µm unless stated otherwise) were collected throughout the hippocampus, immunolabeled and imaged using a 5× or a 10× objective. The number of cells of interest was scored using the Cell Counter plugin, ImageJ (NIH) as described previously (Chen et al., 2015; De Gregorio et al., 2020). For quantification of *Thy1-GFP/M*-expressing neurons in the CA1, *Thy1-GFP/M* was first crossed into $SERT^{fl/fl}$ mice and *Thy1-GFP/M;*$SERT^{fl/fl}$ mice were then used to generate *Thy1-GFP/M;* $SERT^{PyramidΔ}$ and control *Thy1-GFP/M;*$SERT^{fl/fl}$ littermate mice. The brains of $SERT^{PyramidΔ}$ mice and littermate controls were processed in parallel and compared. Images of the hippocampal structure were tiled using ImageJ, and the number of GFP^+ cells in the entire CA1 region on both hippocampi on 90 µm sections over 18, 21 and 22 consecutive sections was counted for P3, P6 and P16, respectively, starting from the hippocampal commissure. For quantification of the percentage of $SERT^{Cre/+}$-dependent tdTom-expressing neurons in CA3a, CA3b and CA3c subfields, two sections each from dorsal and ventral hippocampus were analyzed for each $SERT^{Cre/+}$*;Ai14* mouse, and the number of $tdTom^+$ neurons and DAPI counterstained cell nuclei over a defined region of interest (ROI) in the pyramidal layer within each CA3 subfield was counted. For all other cell counts, every other section starting from the hippocampal commissure was stained for one set of antibodies. For each brain, both the left and right dorsal hippocampus in six sections were scored and the average is reported in the graphs.

BrdU labeling was used to assess the birth of *Thy1-GFP/M*-expressing neurons located in the CA1 and DG. To mark embryonic neurogenesis, a single pulse of BrdU (MP Biomedicals 100171) was administrated intraperitoneally into dams at 25 µg/g body weight at E14.5, E16.5 and E18.5. The date of birth of the pups was considered as P0. To label neurons generated postnatally, BrdU was injected into pups at 100 µg/g body weight. To visualize BrdU labeling, 75 µm serial coronal sections were collected from P16 mice that had been exposed to BrdU embryonically or postnatally, and every other section was stained with anti-BrdU and anti-GFP antibodies. For each brain, four sections corresponding to the middle dorsal hippocampus were analyzed. All $BrdU^+/GFP^+$ and $BrdU^-/GFP^+$ neurons in the CA1 area on the sections were scored. Because of the high density of GFP^+ cells in the DG, the number of $BrdU^+/GFP^+$ and $BrdU^-/GFP^+$ neurons in a defined region of interest (ROI) (430 µm×340 µm) at the far end of suprapyramidal blade of the DG were scored and reported in the graphs.

In situ hybridization

Mice were anesthetized, sacrificed and brains fixed as for immunohistochemistry analyses. Post-fixed brains were cryoprotected through two consecutive 24 h and 48 h steps at 4°C in diethylpyrocarbonate (DEPC, Sigma D5758)-treated PBS containing 15% and 30% sucrose, respectively, and frozen in optimal cutting temperature (OCT, Sakura 4583). Sections (20 µm) were cut on a cryostat (Leica) and stored at −80°C until use. *In situ* hybridization was performed using the specific *Mus musculus Slc6a4* probe (ACD, RNAscope Probe - Mm-*Slc6a4*, 315851) and the RNAscope 2.5 HD Detection Kit (Red Assay, ACD 322350) following the user manual instructions, with the only difference being that sections were counterstained with DAPI rather than Hematoxylin.

AAV-mediated anterograde tracing of SERT-expressing projections

The virus AAV1.CAG.Flex.eGFP.WPRE.bGH (Allen Institute 854, Penn Vector Core, University of Pennsylvania, Philadelphia, PA, USA) was used in whole-brain tracing of SERT-expressing hippocampal and mPFC neuron axonal projections in $SERT^{Cre/+}$ mice. P5 $SERT^{Cre/+}$ pups were cryoanesthetized on ice, and placed on a hypothermic mouse neonatal stereotaxic adaptor (Stoelting, 51625M) to maintain a low pup body temperature during surgery, with the head fixed through the apparatus head stabilizers. The coordinates were based upon the Atlas of the Developing Mouse Brain (Paxinos et al., 2006) with the skull surface set as 0 along the DV axis, the sagittal sinus as 0 along ML axis and the bregma as 0 along the AP axis. The coordinates in mm for the hippocampal injection were −0.96 AP, 2.12 ML, −1.78DV and +1.56 AP, 0.29 ML, −1.79 DV for the mPFC. Unilateral injection of 300 nl of AAV1.CAG.Flex.eGFP.WPRE.bGH ($2.96×10^{12}$ GC/ml) was delivered at the rate of 100 nl/min, using a Hamilton syringe (65460-03) carrying a 33 gauge needle and loaded on a microinjection syringe pump (WPI, UMP3T-1). Pups were then recovered on a heated pad, returned to mothers and analyzed at P18. For tracing, post-fixed brains were cut into serial 90 µm vibratome sections, stained with anti-GFP antibody, counterstained with DAPI and images were acquired sequentially using Zeiss Axio Scan Z.1 slide scanner, which automatically generates tiled images of individual tissue sections. Eighteen and 16 pups were injected for anterograde tracing of hippocampal and mPFC SERT-expressing neurons, respectively, and the best six successful injections (three females and three males for the mPFC injection and two females and four males for the hippocampal injection) were analyzed.

Spine morphometric analyses and dendritic tree reconstructions

For both spine morphometric analyses and dendritic tree reconstructions, the brains of *Thy1-GFP/M;*$SERT^{PyramidΔ}$ mice and control *Thy1-GFP/M;* $SERT^{fl/fl}$ littermates were processed in parallel and compared. Animals were perfused and brains post-fixed as described for immunohistochemistry analyses. Vibratome sections (120 µm and 250 µm) were used for spine morphometric analyses and CA1 pyramidal neuron apical dendritic tree reconstruction, respectively. The immunostaining protocol was adjusted to allow a deeper penetrance of antibody. Specifically, the percentage of Triton X-100 was increased to 0.5% in solutions for permeabilization, blocking and anti-GFP antibody incubation, and anti-GFP incubation was carried out overnight at 37°C for 120 µm sections, and for 60 h at 37°C for 250 µm sections in a humified chamber to avoid sections being dried. Secondary

Development (2022) 149, dev200549. doi:10.1242/dev.200549

antibody incubation time was increased to 3 h at room temperature. Sections were counterstained with DAPI.

For the spine morphometric analyses, 50 µm long, 3rd order GFP$^+$ dendritic segments in the stratum radiatum corresponding to the middle third of CA1 along the proximodistal axis of dorsal hippocampus were randomly selected. Segments were acquired on a Zeiss AiryScan LSM880 confocal microscope set at the Superresolution mode using a 63× (NA 1.4) oil-immersion objective. *Z*-stack acquisitions with an optimal *z*-stack step of 0.19 µm were made to acquire the 50 µm long central region of the segment, with a 2× digital zoom and a frame size of 1560×1560 pixel, resulting in a voxel size of 0.4×0.4×0.19 µm^3. The acquired images were converted to the OME.TIFF format through the Bio-Formats plug-in on ImageJ and imported into the Imaris software (Bitplane) for semi-automatic spine morphometric analyses. The starting and ending points for each segment were manually assigned in order to avoid scoring regions within 20 µm of the branching or ending points. For the spine detection, preset parameters were used, the seed point threshold was manually defined, and spines volume, diameter, length and general spine density were automatically computed. The density of thin and mushroom spines of each dendritic segment was manually scored using the Cell Counter plug-in (ImageJ) as described previously (Speranza et al., 2017), according to the criteria set by the classic work of Harris and colleagues (Harris et al., 1992). Briefly, the length of spine (the distance from spine emerging point on the dendrite to its tip) and the head diameter were measured using the line tool on ImageJ, and dendritic spines with a length greater than the neck diameter and the neck diameter similar to the head diameter were judged as thin type, while spines showing a head diameter much greater than the neck diameter were counted as mushroom type.

For the CA1 pyramidal neuron apical dendritic tree reconstruction, neurons within the same middle third area of the CA1 for spine characterization were randomly selected. Individual neurons were imaged on a Zeiss LSM 5DUO confocal microscope using a 25× (NA 0.8) Imm Korr objective. Using the combination of a two-tiles acquisition, no digital zoom, with a *z*-stack encompassing 50 µm to 65 µm of the section, the entire apical dendritic tree was acquired. Acquisitions were made with a *z*-step of 2.15 µm, frame size of 4338×2284, resulting in a voxel size of 0.15×0.15×2.15 µm^3. Acquired images were imported into the Neurolucida software (MBF Bioscience) for semi-automatic tracing, for three-dimensional reconstruction of the apical dendritic tree, and for quantification of branch length and the number of branch point, segments and endings. In addition, Sholl analyses (Sholl, 1953) were performed and showed no major tree organization alterations in *SERT*$^{fl/fl}$ versus *SERT*^{PyramidΔ} mice (15 neurons from three *SERT*$^{fl/fl}$ mice and 16 neurons from three *SERT*^{PyramidΔ} mice; R.D.G., unpublished).

Behavioral tests

The same cohort of mice (11 *SERT*$^{fl/fl}$ males, 14 *SERT*^{PyramidΔ} males, 15 *SERT*$^{fl/fl}$ females and 12 *SERT*^{PyramidΔ} females; 19±3 weeks of age) was used for all the behavioral assays except for the FST. The first behavioral test was EPM, followed by open field, social interaction and contextual fear conditioning, with intervals of least 5 days between the tests. Because of the severe stress from forced swimming, FST was performed with another cohort that comprised 18 *SERT*$^{fl/fl}$ males, 19 *SERT*^{PyramidΔ} males, 17 *SERT*$^{fl/fl}$ females and 17 *SERT*^{PyramidΔ} females (18±3 weeks old). All tests were performed between 9:00 AM and 5:00 PM in a dedicated room under white light (unless stated otherwise). Mice were handled 1 day before each test and allowed to acclimate to the room for at least 1 h before testing. For all tests, trial orders were pre-assigned to counterbalance for genotypes across session (morning, afternoon) and for the chamber-sides in social behavioral tests, and the experimenters were blinded to animal genotypes. Testing apparatus was cleaned with 70% ethanol after every trial.

Forced swimming test

Each mouse was placed for 5 min in a glass cylinder (18 cm in diameter×24 cm height) filled with water to 15 cm height maintained at 18°C. Behavior was recorded and the time spent immobile (when the animal was in a passive floating condition or displaying only slight movements with one of the hindlimbs) scored.

Elevated plus maze test

The elevated plus maze (EPM) consists of two enclosed arms (50 cm length×10 cm width×40 cm height) with opaque perspex walls and two open arms (50 cm length×10 cm width) with small 2 cm tall rails, elevated 50 cm above the floor. Mice were placed at the center of the apparatus and allowed to move freely for a 10-min testing session under red light. Behavior was tracked and scored using the Viewer tracking software (Biobserve). Scored parameters were: total and percentage of time spent in the open/closed arms, total and percentage of travelled distance in the open/closed arms, the number of entries to the open/closed arms and total travelled distance.

Open field test

Mice were placed in an opaque plexiglass box (38 cm width×38 cm length×38 cm height) illuminated with a bulb placed exactly above the apparatus and allowed to explore freely for a 10 min testing session. Behavior was recorded, and travelled distance tracked and scored using the AnyMaze tracking software (Stoelting). Scored parameters were: total and the percentage of time spent in the central squared arena (16 cm×16 cm), the number of entries into the center arena, mean distance from the center point of the apparatus and total travelled distance.

Social interaction and novelty tests

Three-chamber social interaction and novelty tests comprised three 9-min sessions: habituation, social interaction and social novelty. Unfamiliar mice for both the social interaction and social novelty tests were age- and sex-matched *SERT*$^{fl/fl}$ mice. The apparatus was a rectangular, three-chamber plexiglass box (each chamber being 20 cm×40 cm) with opaque external walls and two clear dividing walls, each with a small doorway to allow access to the side chambers. During the habituation phase, the mouse was placed in the center chamber and allowed to explore the entire empty apparatus. For the interaction session, the test mouse was placed in the middle chamber with the doors closed. A wire cup containing an unfamiliar mouse was placed in one side chamber, while an empty wire cup was placed in the opposite side chamber. The locations of the mouse and the empty cup were alternated between left and right after each trial to exclude side preference. The doors were then lifted simultaneously, allowing the test mouse to freely explore all three chambers. For the social novelty session, the test mouse was placed into the middle chamber with the doors to both side chambers closed. The previously empty cup was filled with a novel unfamiliar mouse, and the doors lifted, to allow the test mouse to explore all the three chambers freely and choose between the two mice. Behavior was recorded, and the paths were tracked and scored using the AnyMaze tracking software. Scored parameters were: total and percentage of time spent in each of the chambers, distance travelled in each of the chambers and the number of entries to the two side chambers. In order to perform two-way ANOVA, the social preference and novelty indexes were calculated as $I=(T_S-T_{NS})/(T_S+T_{NS})$, with T_S being the time spent in the mouse or novel mouse chamber and T_{NS} the time spent in the empty or familiar mouse chamber, respectively (Walsh et al., 2018).

Contextual fear conditioning

Contextual fear conditioning was performed in a conditioning chamber (18 cm×20 cm×28 cm) with a metal grid floor inside a sound-attenuated cubicle (Coulbourn Instruments). The grid was connected to a shocker (Coulbourn Instruments) for delivery of electric foot shocks. On training day, individual mice were allowed to freely explore the chamber for 150 s, after which three electric footshocks (0.6 mA for 2 s, with 60 s intervals) were delivered. The mice remained in training chamber for another 30 s and then returned to home cages. The context test was performed every day for the next 10 days after the training. Each day, individual mice were placed back into the conditioning chamber for 4 min without shock, and the freezing and locomotor activity were scored using the Actimetrics FreezeFrame software (Coulbourn Instruments). The grid floor was cleaned with 5% acetic acid after every trial.

Acute slice preparation and electrophysiology

Electrophysiological field potential recording from Schaffer collateral-CA1 synapses in hippocampal slices from *SERT*^{PyramidΔ} and *SERT*$^{fl/fl}$ littermate

Development (2022) 149, dev200549. doi:10.1242/dev.200549

mice, 7-8 weeks of age, were performed as described previously (Miry et al., 2021; Stanton et al., 2003). Mice were decapitated under deep isoflurane anesthesia, and the hippocampus plus entorhinal cortex dissected free from surrounding tissue and placed immediately in ice-cold artificial cerebrospinal fluid (aCSF) consisting of: 126 mM NaCl, 26 mM $NaHCO_3$, 1.25 mM NaH_2PO_4, 5 mM KCl, 2 mM $CaCl_2$, 2 mM $MgCl_2$, and 10 mM D-glucose, continuously gassed with 95% O_2/5% CO_2 (pH 7.2-7.4). Transverse slices (400 µm) were cut using a vibrating tissue slicer (VT1200S, Leica Biosystems). Slices were allowed to recover for 1 h at room temperature in aCSF, before transfer to an interface recording chamber at 33°C and continuously perfusion with aCSF (3 ml/min), where they were incubated for a minimum of 30 min before the start of recording. Extracellular population fEPSP recordings were made using glass microelectrodes (2–3 MΩ filled with aCSF) placed in the stratum radiatum of the CA1 region of hippocampal slices under visual guidance, to a depth of 100-150 µm. Bipolar stainless-steel stimulation electrodes (FHC) were placed in the stratum radiatum to activate Schaffer collateral afferents. For baseline recordings, synaptic inputs were stimulated once each 30 s (150 µs square DC pulse). Baseline stimulus strength (10-200 µA) was adjusted to elicit a response ≈50% of the maximum fEPSP amplitude before the generation of a population action potential, and monitored for at least 30 min before induction of LTP (two theta burst trains of 10×5 pulses at 100 Hz, given 3 min apart, with this pair repeated three times at 15 min intervals) or LTD (2 Hz/10 min). Slices in which there was a drift in baseline of >5% for the 5 min before high-frequency stimulation were excluded from further analysis. Synaptic strength was quantified by measuring the maximum slope of the initial falling phase of the fEPSP, using a six-point interpolation least-squares linear regression analysis, which marched along the response until the maximum value was retrieved. Signals were collected with an Axoclamp-2A amplifier (Molecular Devices) filtered at 1 kHz, sampled at 10 kHz, and digitized and analyzed using DataWave Technologies software (DataWave).

RNA-Seq and analyses

RNA-Seq was performed on mRNA extracted from dorsal hippocampal tissue dissected from P7 *SERT*$^{Pyramid\Delta}$ and *SERT*$^{fl/fl}$ pups in three replicates; each replicate consisted of dorsal hippocampi from four mice. mRNA libraries were prepared using the Illumina Truseq RNA Library Prep Kit V2 (RS-122-2001) on 250 ng total RNA and sequenced on the Illuminia Novaseq platform. FastQC (Version 0.72) was performed on the concatenated replicate raw sequencing reads from each library to ensure minimal PCR duplication and sequencing quality. Reads were aligned to the mm10genome using HISAT2 (version 2.1.0) and annotated against Ensembl v90. Multiple-aligned reads were removed, and remaining transcript reads were counted using featurecounts (Version 2.0.1). DESEQ2 (Love et al., 2014) (Version 2.11.40.6) was then used to normalize read counts between four groups, and to perform pairwise differential expression analyses. Functional annotation analyses using DAVID software (DAVID Bionformatic Resources 6.8, https://david.ncifcrf.gov) (Huang et al., 2009) and the Ingenuity Pathway Analyses software (Qiagen) were performed on differentially expressed protein-coding genes (PCGs) with nominal *P* values of ≤0.05, ≤0.01 and ≤0.005. In Fig. 6B, the -$\log_{10}$ of the EASE score obtained through DAVID, a modified Fisher Exact test *P* value, is plotted in the graphs for each GO term. For gene set enrichment analyses against cell type-specific markers, we used the neuron, astrocyte and oligodendrocyte gene lists from Cahoy et al. (2008), with non-PCGs and genes not present in our dataset filtered out. ASD risk genes were from the human gene module list and genes classified as syndromic curated in the SFARI Gene Autism Database (gene.sfari.org). The odds ratio for the enrichment was calculated as the ratio of B/D to A/C, where A is the non-in set DEGs, B is the in set DEGs, C is non-in set non-DEGs and D is in set non-DEGs.

For RT-qPCR validation experiments, total RNA was extracted from dorsal hippocampal tissue dissected from P7 *SERT*$^{Pyramid\Delta}$ and *SERT*$^{fl/fl}$ pups in three replicates; each replicate contained dorsal hippocampi from four mice. The extraction was performed using Trizol (Thermo Fisher, 15596026)-chloroform, followed by cleanup and elution into RNAse-free water using the RNeasy Minelute Cleanup kit (Qiagen, 74204), as per manufacturer's instructions. Total RNA (500 ng) was used for the cDNA synthesis through the SuperScript VILO IV Master Mix kit (Thermo Fisher, 11766050). qPCR was performed in triplicate on 4 µl of diluted cDNA (1:50) using Power SYBR Green Master Mix (Thermo Fisher, 4367659), in the presence of 0.5 µM of a specific oligo couple. Data were normalized to Gapdh, Hmbs and Ywhaz housekeeping genes. Oligo sequences are listed in Table S12.

SDS PAGE and western blotting

P7 dorsal hippocampal samples were collected as for the RNA-Seq and RT-qPCR experiments. Sample lysis was performed in RIPA buffer [50 mM Tris-HCl (pH 8), 150 mM NaCl, 1% IGEPAL CA-630, 0.5% sodium deoxycholate and 0.1% SDS) supplemented with protease and phosphatase inhibitors (7× Complete proteinase and 10× PhosStop phosphatase inhibitor cocktails – Millipore-Sigma/Roche 11697498001 and 4906845001; 0.5 mM PMSF, 1 mM DDT, 1 mM EGTA, 2 mM NaF, 1 µM microcystine, 1 mM benzamidine hydrochloride and 1 mM sodium orthovanadate). Homogenates were further sonicated in three 10-s pulse-rest cycles, centrifugated for 20 min at 10,000 ***g*** at 4°C and supernatant was collected. Protein concentration was determined using the Biorad DC Protein Assay Kit (Biorad, 5000111) and concentration read using a Nanodrop 2000c, with cuvette capability. 10 µg of protein were loaded per lane in 1× Laemmli Sample buffer (BioRad, 1610747) on precast 4-15% polyacrylamide gels (BioRad, 4561086), separated and transferred to a PDVF membrane (Millipore, IPVH00010). Membranes were blocked for 1 h in 5% bovine serum albumin (Goldbio, A-420-50) or in 5% non-fat milk (Lab Scientific bioKemix, M0841) in Tris-buffered saline Tween-20 [TBST, 0.1% Tween, 150 mM NaCl and 20 mM Tris-HCl (pH 7.4)] and probed overnight at 4°C in blocking solution with the following antibodies: rabbit anti-pERK1/2 (1:3500, Cell Signaling 9101), rabbit anti-ERK1/2 (1:2000, Cell Signaling 4695), rabbit anti-pMEK1/2 (1:2500, Cell Signaling 9121), mouse anti-MEK1/2 (1:2500, Cell Signaling 4694), mouse anti-β-actin (1:20000, Cell Signaling 3700). After 3×5 min washes in TBST, 1 h incubation at room temperature with horseradish peroxidase (HRP)-conjugated secondary antibodies (1:8000-1:20,000, Jackson ImmunoResearch Labs 111-035-045 and 115-035-062) and 4×10 min washes in TBST, membranes were incubated with the chemiluminescent HRP substrate (Pierce, 32106) for 5 min to be visualized on autoradiographic films (Santa Cruz, sc-201697). The relative protein levels were assessed using the Analyze>Gels tool on ImageJ. Where same membranes were reprobed, a 15-min incubation step at room temperature in stripping buffer (Thermo Scientific, 21059) was performed.

Statistical analyses

Sample size was not predetermined using any statistical method but based on previously published studies using similar approaches with equivalent sizes and showing the power to detect significant statistical differences. For all the experiments, animals were randomly assigned to experimental groups, mutant and control littermates processed and analyzed in parallel, and the experimenters were blinded to the genotypes. Statistical analyses were performed using GraphPad Prism (GraphPad software, v9), with the exception of the mixed effect model, which was conducted using the nlme package on R applied to analyze datasets of the fear conditioning tests. For FST, EPM and open field, both two-tailed unpaired *t*-test and two-way ANOVA followed by Šidák post-hoc analyses were performed. The social interaction and social novelty assays were analyzed using two-tailed paired *t*-test. As an alternative, a social index for each of the two parameters was calculated as described above and a two-way ANOVA followed by Šidák post-hoc test was performed. For the paired pulse facilitation experiment, two-way repeated-measures ANOVA was used with no need for a multiple comparison due to the lack of statistical significance. For qPCR analyses, two-way ANOVA followed by Tukey or Šidák post-hoc analyses were performed. For the gene set over-representation analyses, a two-sided Fisher's exact test was used to evaluate the enrichment. All other experiments were analyzed through two-tailed unpaired *t*-test. Analyses were carried out after determination of the normal distribution and similar variance among the compared groups. Differences were considered statistically significant at $P \leq 0.05$.

Acknowledgements
We thank Dr Tao Wang for professional guidance on statistical analyses and Dr Jean Hebert for sharing the Ai14 mouse line. Confocal microscopy and slide-scanner imaging were performed at the Einstein NECI core supported by the National Institutes of Health (S10OD025295).

Competing interests
The authors declare no competing or financial interests.

Author contributions
Conceptualization: R.D.G., I.M., P.K.S., J.Y.S.; Methodology: R.D.G., G.S., J.C.C., L. Speranza, X.Z., A.R., L. Shen, I.M., P.K.S., J.Y.S.; Validation: R.D.G., G.S., J.C.C., L. Speranza, X.Z., I.M., P.K.S., J.Y.S.; Formal analysis: R.D.G., G.S., J.C.C., L. Speranza, X.Z., A.R., I.M., J.Y.S.; Investigation: R.D.G., L. Speranza, J.Y.S.; Resources: I.M., P.K.S., J.Y.S.; Data curation: R.D.G., G.S., J.C.C., L. Speranza, X.Z., A.R., I.M., P.K.S., J.Y.S.; Writing - original draft: R.D.G., G.S., J.C.C., L. Speranza, X.Z., I.M., P.K.S., J.Y.S.; Writing - review & editing: R.D.G., L. Speranza, I.M., P.K.S., J.Y.S.; Supervision: L. Shen, I.M., P.K.S., J.Y.S.; Project administration: I.M., P.K.S., J.Y.S.; Funding acquisition: I.M., J.Y.S.

Funding
This work was supported by the National Institutes of Health (R01MH116900 to I.M., and R56MH105839 and R01MH105839 to J.Y.S.). Deposited in PMC for release after 12 months.

Data availability
The RNA-seq datasets for male and female *SERTP*$^{yramid\Delta}$ and control hippocampus have been deposited in GEO under accession number GSE214392.

Peer review history
The peer review history is available online at https://journals.biologists.com/dev/lookup/doi/10.1242/dev.200549.reviewer-comments.pdf

References

Abel, K. M., Drake, R. and Goldstein, J. M. (2010). Sex differences in schizophrenia. *Int. Rev. Psychiatry* **22**, 417-428. doi:10.3109/09540261.2010.515205

Albert-Gascó, H., Ros-Bernal, F., Castillo-Gómez, E. and Olucha-Bordonau, F. E. (2020). MAP/ERK signaling in developing cognitive and emotional function and its effect on pathological and neurodegenerative processes. *Int. J. Mol. Sci.* **21**, 4471. doi:10.3390/ijms21124471

Altman, J. and Bayer, S. A. (1990). Prolonged sojourn of developing pyramidal cells in the intermediate zone of the hippocampus and their settling in the stratum pyramidale. *J. Comp. Neurol.* **301**, 343-364. doi:10.1002/cne.903010303

Altman, J. and Das, G. D. (1966). Autoradiographic and histological studies of postnatal neurogenesis. I. A longitudinal investigation of the kinetics, migration and transformation of cells incorporating tritiated thymidine in neonate rats, with special reference to postnatal neurogenesis in some brain regions. *J. Comp. Neurol.* **126**, 337-389. doi:10.1002/cne.901260302

Ansorge, M. S., Zhou, M., Lira, A., Hen, R. and Gingrich, J. A. (2004). Early-life blockade of the 5-HT transporter alters emotional behavior in adult mice. *Science* **306**, 879-881. doi:10.1126/science.1101678

Auerbach, B. D., Osterweil, E. K. and Bear, M. F. (2011). Mutations causing syndromic autism define an axis of synaptic pathophysiology. *Nature* **480**, 63-68. doi:10.1038/nature10658

Azmitia, E. C. (1999). Serotonin neurons, neuroplasticity, and homeostasis of neural tissue. *Neuropsychopharmacology* **21**, 33S-45S. doi:10.1016/S0893-133X(99)00022-6

Bale, T. L., Baram, T. Z., Brown, A. S., Goldstein, J. M., Insel, T. R., McCarthy, M. M., Nemeroff, C. B., Reyes, T. M., Simerly, R. B., Susser, E. S. et al. (2010). Early life programming and neurodevelopmental disorders. *Biol. Psychiatry* **68**, 314-319. doi:10.1016/j.biopsych.2010.05.028

Bayer, S. A. (1980). Development of the hippocampal region in the rat. II. Morphogenesis during embryonic and early postnatal life. *J. Comp. Neurol.* **190**, 115-134. doi:10.1002/cne.901900108

Berry, K. P. and Nedivi, E. (2017). Spine dynamics: are they all the same? *Neuron* **96**, 43-55. doi:10.1016/j.neuron.2017.08.008

Berumen, L. C., Rodríguez, A., Miledi, R. and García-Alcocer, G. (2012). Serotonin receptors in hippocampus. *Scie. World J.* **2012**, 823493. doi:10.1100/2012/823493

Bonnin, A. and Levitt, P. (2011). Fetal, maternal, and placental sources of serotonin and new implications for developmental programming of the brain. *Neuroscience* **197**, 1-7. doi:10.1016/j.neuroscience.2011.10.005

Buznikov, G. A., Lambert, W. H. and Lauder, J. M. (2001). Serotonin and serotonin-like substances as regulators of early embryogenesis and morphogenesis. *Cell Tissue Res.* **305**, 177-186. doi:10.1007/s004410100408

Cadwell, C. R., Bhaduri, A., Mostajo-Radji, M. A., Keefe, M. G. and Nowakowski, T. J. (2019). Development and arealization of the cerebral cortex. *Neuron* **103**, 980-1004. doi:10.1016/j.neuron.2019.07.009

Cahoy, J. D., Emery, B., Kaushal, A., Foo, L. C., Zamanian, J. L., Christopherson, K. S., Xing, Y., Lubischer, J. L., Krieg, P. A., Krupenko, S. A. et al. (2008). A transcriptome database for astrocytes, neurons, and oligodendrocytes: a new resource for understanding brain development and function. *J. Neurosci.* **28**, 264-278. doi:10.1523/JNEUROSCI.4178-07.2008

Canli, T. and Lesch, K.-P. (2007). Long story short: the serotonin transporter in emotion regulation and social cognition. *Nat. Neurosci.* **10**, 1103-1109. doi:10.1038/nn1964

Caspi, A., Hariri, A. R., Holmes, A., Uher, R. and Moffitt, T. E. (2010). Genetic sensitivity to the environment: the case of the serotonin transporter gene and its implications for studying complex diseases and traits. *Am. J. Psychiatry* **167**, 509-527. doi:10.1176/appi.ajp.2010.09101452

Chen, X., Ye, R., Gargus, J. J., Blakely, R. D., Dobrenis, K. and Sze, J. Y. (2015). Disruption of transient serotonin accumulation by non-serotonin-producing neurons impairs cortical map development. *Cell Rep.* **10**, 346-358. doi:10.1016/j.celrep.2014.12.033

Chen, X., Petit, E. I., Dobrenis, K. and Sze, J. Y. (2016). Spatiotemporal SERT expression in cortical map development. *Neurochem. Int.* **98**, 129-137. doi:10.1016/j.neuint.2016.05.010

Colgan, L. A., Putzier, I. and Levitan, E. S. (2009). Activity-dependent vesicular monoamine transporter-mediated depletion of the nucleus supports somatic release by serotonin neurons. *J. Neurosci.* **29**, 15878-15887. doi:10.1523/JNEUROSCI.4210-09.2009

Collado-Torres, L., Burke, E. E., Peterson, A., Shin, J. H., Straub, R. E., Rajpurohit, A., Semick, S. A., Ulrich, W. S., Price, A. J., Valencia, C. et al. (2019). Regional heterogeneity in gene expression, regulation, and coherence in the frontal cortex and hippocampus across development and Schizophrenia. *Neuron* **103**, 203-216.e208. doi:10.1016/j.neuron.2019.05.013

Cote, F., Fligny, C., Bayard, E., Launay, J.-M., Gershon, M. D., Mallet, J. and Vodjdani, G. (2007). Maternal serotonin is crucial for murine embryonic development. *Proc. Natl. Acad. Sci. USA* **104**, 329-334. doi:10.1073/pnas.0606722104

De Gregorio, R., Chen, X., Petit, E. I., Dobrenis, K. and Sze, J. Y. (2020). Disruption of transient SERT expression in thalamic glutamatergic neurons alters trajectory of postnatal interneuron development in the mouse cortex. *Cereb. Cortex* **30**, 1623-1636. doi:10.1093/cercor/bhz191

Deguchi, Y., Donato, F., Galimberti, I., Cabuy, E. and Caroni, P. (2011). Temporally matched subpopulations of selectively interconnected principal neurons in the hippocampus. *Nat. Neurosci.* **14**, 495-504. doi:10.1038/nn.2768

Dölen, G., Osterweil, E., Rao, B. S. S., Smith, G. B., Auerbach, B. D., Chattarji, S. and Bear, M. F. (2007). Correction of fragile X syndrome in mice. *Neuron* **56**, 955-962. doi:10.1016/j.neuron.2007.12.001

Eblen, S. T. (2018). Extracellular-regulated kinases: signaling from Ras to ERK substrates to control biological outcomes. *Adv. Cancer Res.* **138**, 99-142. doi:10.1016/bs.acr.2018.02.004

Farrelly, L. A., Thompson, R. E., Zhao, S., Lepack, A. E., Lyu, Y., Bhanu, N. V., Zhang, B., Loh, Y.-H. E., Ramakrishnan, A., Vadodaria, K. C. et al. (2019). Histone serotonylation is a permissive modification that enhances TFIID binding to H3K4me3. *Nature* **567**, 535-539. doi:10.1038/s41586-019-1024-7

Feng, G., Mellor, R. H., Bernstein, M., Keller-Peck, C., Nguyen, Q. T., Wallace, M., Nerbonne, J. M., Lichtman, J. W. and Sanes, J. R. (2000). Imaging neuronal subsets in transgenic mice expressing multiple spectral variants of GFP. *Neuron* **28**, 41-51. doi:10.1016/S0896-6273(00)00084-2

Garbarino, V. R., Gilman, T. L., Daws, L. C. and Gould, G. G. (2019). Extreme enhancement or depletion of serotonin transporter function and serotonin availability in autism spectrum disorder. *Pharmacol. Res.* **140**, 85-99. doi:10.1016/j.phrs.2018.07.010

Gaspar, P., Cases, O. and Maroteaux, L. (2003). The developmental role of serotonin: news from mouse molecular genetics. *Nat. Rev. Neurosci.* **4**, 1002-1012. doi:10.1038/nrn1256

Geschwind, D. H. and Rakic, P. (2013). Cortical evolution: judge the brain by its cover. *Neuron* **80**, 633-647. doi:10.1016/j.neuron.2013.10.045

Gingrich, J. A., Malm, H., Ansorge, M. S., Brown, A., Sourander, A., Suri, D., Teixeira, C. M., Caffrey Cagliostro, M. K., Mahadevia, D. and Weissman, M. M. (2017). New insights into how serotonin selective reuptake inhibitors shape the developing brain. *Birth Defects Res.* **109**, 924-932. doi:10.1002/bdr2.1085

Glover, M. E. and Clinton, S. M. (2016). Of rodents and humans: a comparative review of the neurobehavioral effects of early life SSRI exposure in preclinical and clinical research. *Int. J. Dev. Neurosci.* **51**, 50-72. doi:10.1016/j.ijdevneu.2016.04.008

Gorski, J. A., Talley, T., Qiu, M., Puelles, L., Rubenstein, J. L. R. and Jones, K. R. (2002). Cortical excitatory neurons and glia, but not GABAergic neurons, are produced in the Emx1-expressing lineage. *J. Neurosci.* **22**, 6309-6314. doi:10.1523/JNEUROSCI.22-15-06309.2002

Hahn, M. K. and Blakely, R. D. (2007). The functional impact of SLC6 transporter genetic variation. *Annu. Rev. Pharmacol. Toxicol.* **47**, 401-441. doi:10.1146/annurev.pharmtox.47.120505.105242

Hansson, S. R., Mezey, É. and Hoffman, B. J. (1998). Serotonin transporter messenger RNA in the developing rat brain: early expression in serotonergic neurons and transient expression in non-serotonergic neurons. *Neuroscience* **83**, 1185-1201. doi:10.1016/S0306-4522(97)00444-2

Harris, K. M., Jensen, F. E. and Tsao, B. (1992). Three-dimensional structure of dendritic spines and synapses in rat hippocampus (CA1) at postnatal day 15 and adult ages: implications for the maturation of synaptic physiology and long-term potentiation. *J. Neurosci.* **12**, 2685-2705. doi:10.1523/JNEUROSCI.12-07-02685.1992

Hensch, T. K. (2004). Critical period regulation. *Annu. Rev. Neurosci.* **27**, 549-579. doi:10.1146/annurev.neuro.27.070203.144327

Hoffman, G. E., Ma, Y., Montgomery, K. S., Bendl, J., Jaiswal, M. K., Kozlenkov, A., CommonMind Consortium, Peters, M. A., Dracheva, S., Fullard, J. F., Chess, A. et al. (2022). Sex differences in the human brain transcriptome of cases with schizophrenia. *Biol. Psychiatry*. **91**, 92-101. doi:10.1101/2020.10.05.326405

Huang, D. W., Sherman, B. T. and Lempicki, R. A. (2009). Bioinformatics enrichment tools: paths toward the comprehensive functional analysis of large gene lists. *Nucleic Acids Res.* **37**, 1-13. doi:10.1093/nar/gkn923

Iwano, T., Masuda, A., Kiyonari, H., Enomoto, H. and Matsuzaki, F. (2012). Prox1 postmitotically defines dentate gyrus cells by specifying granule cell identity over CA3 pyramidal cell fate in the hippocampus. *Development* **139**, 3051-3062. doi:10.1242/dev.080002

Jafari, G., Xie, Y., Kullyev, A., Liang, B. and Sze, J. Y. (2011). Regulation of extrasynaptic 5-HT by serotonin reuptake transporter function in 5-HT-absorbing neurons underscores adaptation behavior in Caenorhabditis elegans. *J. Neurosci.* **31**, 8948-8957. doi:10.1523/JNEUROSCI.1692-11.2011

Jung, H., Park, H., Choi, Y., Kang, H., Lee, E., Kweon, H., Roh, J. D., Ellegood, J., Choi, W., Kang, J. et al. (2018). Sexually dimorphic behavior, neuronal activity, and gene expression in Chd8-mutant mice. *Nat. Neurosci.* **21**, 1218-1228. doi:10.1038/s41593-018-0208-z

Kandel, E. R., Dudai, Y. and Mayford, M. R. (2014). The molecular and systems biology of memory. *Cell* **157**, 163-186. doi:10.1016/j.cell.2014.03.001

Kim, J. J. and Fanselow, M. S. (1992). Modality-specific retrograde amnesia of fear. *Science* **256**, 675-677. doi:10.1126/science.1585183

Lebrand, C., Cases, O., Wehrlé, R., Blakely, R. D., Edwards, R. H. and Gaspar, P. (1998). Transient developmental expression of monoamine transporters in the rodent forebrain. *J. Comp. Neurol.* **401**, 506-524. doi:10.1002/(SICI)1096-9861(19981130)401:4<506::AID-CNE5>3.0.CO;2-#

Lee, F. S., Heimer, H., Giedd, J. N., Lein, E. S., Sestan, N., Weinberger, D. R. and Casey, B. J. (2014). Mental health. Adolescent mental health–opportunity and obligation. *Science* **346**, 547-549. doi:10.1126/science.1260497

Leinekugel, X. (2003). Developmental patterns and plasticities: the hippocampal model. *J. Physiol. Paris* **97**, 27-37. doi:10.1016/j.jphysparis.2003.10.004

Lenz, K. M., Nugent, B. M. and McCarthy, M. M. (2012). Sexual differentiation of the rodent brain: dogma and beyond. *Front. Neurosci.* **6**, 26. doi:10.3389/fnins.2012.00026

Li, M., Santpere, G., Imamura Kawasawa, Y., Evgrafov, O. V., Gulden, F. O., Pochareddy, S., Sunkin, S. M., Li, Z., Shin, Y., Zhu, Y. et al. (2018). Integrative functional genomic analysis of human brain development and neuropsychiatric risks. *Science* **362**, eaat7615. doi:10.1126/science.aat7615

Lim, L., Mi, D., Llorca, A. and Marin, O. (2018). Development and functional diversification of cortical interneurons. *Neuron* **100**, 294-313. doi:10.1016/j.neuron.2018.10.009

Lister, R., Mukamel, E. A., Nery, J. R., Urich, M., Puddifoot, C. A., Johnson, N. D., Lucero, J., Huang, Y., Dwork, A. J., Schultz, M. D. et al. (2013). Global epigenomic reconfiguration during mammalian brain development. *Science* **341**, 1237905. doi:10.1126/science.1237905

Love, M. I., Huber, W. and Anders, S. (2014). Moderated estimation of fold change and dispersion for RNA-seq data with DESeq2. *Genome Biol.* **15**, 550. doi:10.1186/s13059-014-0550-8

Lu, A. T.-H. and Cantor, R. M. (2012). Allowing for sex differences increases power in a GWAS of multiplex Autism families. *Mol. Psychiatry* **17**, 215-222. doi:10.1038/mp.2010.127

Lugo-Candelas, C., Cha, J., Hong, S., Bastidas, V., Weissman, M., Fifer, W. P., Myers, M., Talati, A., Bansal, R., Peterson, B. S. et al. (2018). Associations between brain structure and connectivity in infants and exposure to selective serotonin reuptake inhibitors during pregnancy. *JAMA Pediatr.* **172**, 525-533. doi:10.1001/jamapediatrics.2017.5227

Madisen, L., Zwingman, T. A., Sunkin, S. M., Oh, S. W., Zariwala, H. A., Gu, H., Ng, L. L., Palmiter, R. D., Hawrylycz, M. J., Jones, A. R. et al. (2010). A robust and high-throughput Cre reporting and characterization system for the whole mouse brain. *Nat. Neurosci.* **13**, 133-140. doi:10.1038/nn.2467

Maenner, M. J., Shaw, K. A., Baio, J., Washington, A., Patrick, M., DiRienzo, M., Christensen, D. L., Wiggins, L. D., Pettygrove, S., Andrews, J. G. et al. (2020). Prevalence of autism spectrum disorder among children aged 8 years - autism and developmental disabilities monitoring network, 11 sites, United States, 2016. *MMWR Surveill. Summ.* **69**, 1-12. doi:10.15585/mmwr.ss6904a1

Malm, H., Brown, A. S., Gissler, M., Gyllenberg, D., Hinkka-Yli-Salomäki, S., McKeague, I. W., Weissman, M., Wickramaratne, P., Artama, M., Gingrich, J. A. et al. (2016). Gestational exposure to selective serotonin reuptake inhibitors and offspring psychiatric disorders: a national register-based study. *J. Am. Acad. Child Adolesc. Psychiatry* **55**, 359-366. doi:10.1016/j.jaac.2016.02.013

Marin, O. (2016). Developmental timing and critical windows for the treatment of psychiatric disorders. *Nat. Med.* **22**, 1229-1238. doi:10.1038/nm.4225

McCarthy, M. M. and Arnold, A. P. (2011). Reframing sexual differentiation of the brain. *Nat. Neurosci.* **14**, 677-683. doi:10.1038/nn.2834

McHail, D. G. and Dumas, T. C. (2015). Multiple forms of metaplasticity at a single hippocampal synapse during late postnatal development. *Dev. Cogn. Neurosci.* **12**, 145-154. doi:10.1016/j.dcn.2015.01.009

Miry, O., Zhang, X.-L., Vose, L. R., Gopaul, K. R., Subah, G., Moncaster, J. A., Wojnarowicz, M. W., Fisher, A. M., Tagge, C. A., Goldstein, L. E. et al. (2021). Life-long brain compensatory responses to galactic cosmic radiation exposure. *Sci. Rep.* **11**, 4292. doi:10.1038/s41598-021-83447-y

Mo, A., Mukamel, E. A., Davis, F. P., Luo, C., Henry, G. L., Picard, S., Urich, M. A., Nery, J. R., Sejnowski, T. J., Lister, R. et al. (2015). Epigenomic signatures of neuronal diversity in the mammalian brain. *Neuron* **86**, 1369-1384. doi:10.1016/j.neuron.2015.05.018

Mullins, C., Fishell, G. and Tsien, R. W. (2016). Unifying views of autism spectrum disorders: a consideration of autoregulatory feedback loops. *Neuron* **89**, 1131-1156. doi:10.1016/j.neuron.2016.02.017

Narboux-Neme, N., Pavone, L. M., Avallone, L., Zhuang, X. and Gaspar, P. (2008). Serotonin transporter transgenic (SERTcre) mouse line reveals developmental targets of serotonin specific reuptake inhibitors (SSRIs). *Neuropharmacology* **55**, 994-1005. doi:10.1016/j.neuropharm.2008.08.020

Nowakowski, T. J., Bhaduri, A., Pollen, A. A., Alvarado, B., Mostajo-Radji, M. A., Di Lullo, E., Haeussler, M., Sandoval-Espinosa, C., Liu, S. J., Velmeshev, D. et al. (2017). Spatiotemporal gene expression trajectories reveal developmental hierarchies of the human cortex. *Science* **358**, 1318-1323. doi:10.1126/science.aap8809

Olivier, J. D. A., Åkerud, H., Kaihola, H., Pawluski, J. L., Skalkidou, A., Högberg, U. and Sundström-Poromaa, I. (2013). The effects of maternal depression and maternal selective serotonin reuptake inhibitor exposure on offspring. *Front. Cell Neurosci.* **7**, 73. doi:10.3389/fncel.2013.00073

Paxinos, G., Halliday, G., Watson, C., Koutcherov, Y. and Wang, H. (2006). *Atlas of the Developing Mouse brain at E17.5, P0 and P6*. New York: Academic Press.

Peça, J., Feliciano, C., Ting, J. T., Wang, W., Wells, M. F., Venkatraman, T. N., Lascola, C. D., Fu, Z. and Feng, G. (2011). Shank3 mutant mice display autistic-like behaviours and striatal dysfunction. *Nature* **472**, 437-442. doi:10.1038/nature09965

Peixoto, R. T., Wang, W., Croney, D. M., Kozorovitskiy, Y. and Sabatini, B. L. (2016). Early hyperactivity and precocious maturation of corticostriatal circuits in Shank3B(−/−) mice. *Nat. Neurosci.* **19**, 716-724. doi:10.1038/nn.4260

Persico, A. M., Mengual, E., Moessner, R., Hall, F. S., Revay, R. S., Sora, I., Arellano, J., DeFelipe, J., Giménez-Amaya, J. M., Conciatori, M. et al. (2001). Barrel pattern formation requires serotonin uptake by thalamocortical afferents, and not vesicular monoamine release. *J. Neurosci.* **21**, 6862-6873. doi:10.1523/JNEUROSCI.21-17-06862.2001

Phillips, R. G. and LeDoux, J. E. (1992). Differential contribution of amygdala and hippocampus to cued and contextual fear conditioning. *Behav. Neurosci.* **106**, 274-285. doi:10.1037/0735-7044.106.2.274

Phillips, M. and Pozzo-Miller, L. (2015). Dendritic spine dysgenesis in autism related disorders. *Neurosci. Lett.* **601**, 30-40. doi:10.1016/j.neulet.2015.01.011

Platt, R. J., Zhou, Y., Slaymaker, I. M., Shetty, A. S., Weisbach, N. R., Kim, J.-A., Sharma, J., Desai, M., Sood, S., Kempton, H. R. et al. (2017). Chd8 mutation leads to autistic-like behaviors and impaired striatal circuits. *Cell Rep.* **19**, 335-350. doi:10.1016/j.celrep.2017.03.052

Rakic, P., Ayoub, A. E., Breunig, J. J. and Dominguez, M. H. (2009). Decision by division: making cortical maps. *Trends Neurosci.* **32**, 291-301. doi:10.1016/j.tins.2009.01.007

Sato, D., Lionel, A. C., Leblond, C. S., Prasad, A., Pinto, D., Walker, S., O'Connor, I., Russell, C., Drmic, I. E., Hamdan, F. F. et al. (2012). SHANK1 deletions in males with autism spectrum disorder. *Am. J. Hum. Genet.* **90**, 879-887. doi:10.1016/j.ajhg.2012.03.017

Satterthwaite, T. D., Wolf, D. H., Roalf, D. R., Ruparel, K., Erus, G., Vandekar, S., Gennatas, E. D., Elliott, M. A., Smith, A., Hakonarson, H. et al. (2015). Linked sex differences in cognition and functional connectivity in youth. *Cereb. Cortex* **25**, 2383-2394. doi:10.1093/cercor/bhu036

Scharfman, H. E. (2007). The CA3 "backprojection" to the dentate gyrus. *Prog. Brain Res.* **163**, 627-637. doi:10.1016/S0079-6123(07)63034-9

Schipper, P., Hiemstra, M., Bosch, K., Nieuwenhuis, D., Adinolfi, A., Glotzbach, S., Borghans, B., Lopresto, D., Fernández, G., Klumpers, F. et al. (2019). The association between serotonin transporter availability and the neural correlates of fear bradycardia. *Proc. Natl. Acad. Sci. USA* **116**, 25941-25947. doi:10.1073/pnas.1904843116

Sholl, D. A. (1953). Dendritic organization in the neurons of the visual and motor cortices of the cat. *J. Anat.* **87**, 387-406.
Silbereis, J. C., Pochareddy, S., Zhu, Y., Li, M. and Sestan, N. (2016). The cellular and molecular landscapes of the developing human central nervous system. *Neuron* **89**, 248-268. doi:10.1016/j.neuron.2015.12.008
Soiza-Reilly, M., Meye, F. J., Olusakin, J., Telley, L., Petit, E., Chen, X., Mameli, M., Jabaudon, D., Sze, J.-Y. and Gaspar, P. (2019). SSRIs target prefrontal to raphe circuits during development modulating synaptic connectivity and emotional behavior. *Mol. Psychiatry* **24**, 726-745. doi:10.1038/s41380-018-0260-9
Speranza, L., Labus, J., Volpicelli, F., Guseva, D., Lacivita, E., Leopoldo, M., Bellenchi, G. C., di Porzio, U., Bijata, M., Perrone-Capano, C. et al. (2017). Serotonin 5-HT7 receptor increases the density of dendritic spines and facilitates synaptogenesis in forebrain neurons. *J. Neurochem.* **141**, 647-661. doi:10.1111/jnc.13962
Stanton, P. K., Winterer, J., Bailey, C. P., Kyrozis, A., Raginov, I., Laube, G., Veh, R. W., Nguyen, C. Q. and Müller, W. (2003). Long-term depression of presynaptic release from the readily releasable vesicle pool induced by NMDA receptor-dependent retrograde nitric oxide. *J. Neurosci.* **23**, 5936-5944. doi:10.1523/JNEUROSCI.23-13-05936.2003
Stiles, J. and Jernigan, T. L. (2010). The basics of brain development. *Neuropsychol. Rev.* **20**, 327-348. doi:10.1007/s11065-010-9148-4
Sugiyama, T., Osumi, N. and Katsuyama, Y. (2014). A novel cell migratory zone in the developing hippocampal formation. *J. Comp. Neurol.* **522**, 3520-3538. doi:10.1002/cne.23621
Sze, J. Y., Victor, M., Loer, C., Shi, Y. and Ruvkun, G. (2000). Food and metabolic signalling defects in a Caenorhabditis elegans serotonin-synthesis mutant. *Nature* **403**, 560-564. doi:10.1038/35000609
Tang, G., Gudsnuk, K., Kuo, S.-H., Cotrina, M. L., Rosoklija, G., Sosunov, A., Sonders, M. S., Kanter, E., Castagna, C., Yamamoto, A. et al. (2014). Loss of mTOR-dependent macroautophagy causes autistic-like synaptic pruning deficits. *Neuron* **83**, 1131-1143. doi:10.1016/j.neuron.2014.07.040
Velmeshev, D., Schirmer, L., Jung, D., Haeussler, M., Perez, Y., Mayer, S., Bhaduri, A., Goyal, N., Rowitch, D. H. and Kriegstein, A. R. (2019). Single-cell genomics identifies cell type-specific molecular changes in autism. *Science* **364**, 685-689. doi:10.1126/science.aav8130
Voineagu, I., Wang, X., Johnston, P., Lowe, J. K., Tian, Y., Horvath, S., Mill, J., Cantor, R. M., Blencowe, B. J. and Geschwind, D. H. (2011). Transcriptomic analysis of autistic brain reveals convergent molecular pathology. *Nature* **474**, 380-384. doi:10.1038/nature10110
Walsh, J. J., Christoffel, D. J., Heifets, B. D., Ben-Dor, G. A., Selimbeyoglu, A., Hung, L. W., Deisseroth, K. and Malenka, R. C. (2018). 5-HT release in nucleus accumbens rescues social deficits in mouse autism model. *Nature* **560**, 589-594. doi:10.1038/s41586-018-0416-4
Wamsley, B. and Fishell, G. (2017). Genetic and activity-dependent mechanisms underlying interneuron diversity. *Nature reviews. Neuroscience* **18**, 299-309. doi:10.1038/nrn.2017.30
Werling, D. M., Parikshak, N. N. and Geschwind, D. H. (2016). Gene expression in human brain implicates sexually dimorphic pathways in autism spectrum disorders. *Nat. Commun.* **7**, 10717. doi:10.1038/ncomms10717
Willsey, A. J., Sanders, S. J., Li, M., Dong, S., Tebbenkamp, A. T., Muhle, R. A., Reilly, S. K., Lin, L., Fertuzinhos, S., Miller, J. A. et al. (2013). Coexpression networks implicate human midfetal deep cortical projection neurons in the pathogenesis of autism. *Cell* **155**, 997-1007. doi:10.1016/j.cell.2013.10.020
Wirth, A., Holst, K. and Ponimaskin, E. (2017). How serotonin receptors regulate morphogenic signalling in neurons. *Prog. Neurobiol.* **151**, 35-56. doi:10.1016/j.pneurobio.2016.03.007
Workman, A. D., Charvet, C. J., Clancy, B., Darlington, R. B. and Finlay, B. L. (2013). Modeling transformations of neurodevelopmental sequences across mammalian species. *J. Neurosci.* **33**, 7368-7383. doi:10.1523/JNEUROSCI.5746-12.2013
Zhao, S., Chuh, K. N., Zhang, B., Dul, B. E., Thompson, R. E., Farrelly, L. A., Liu, X., Xu, N., Xue, Y., Roeder, R. G. et al. (2021). Histone H3Q5 serotonylation stabilizes H3K4 methylation and potentiates its readout. *Proc. Natl. Acad. Sci. USA* **118**, e2016742118. doi:10.1073/pnas.2016742118
Zhuang, X., Masson, J., Gingrich, J. A., Rayport, S. and Hen, R. (2005). Targeted gene expression in dopamine and serotonin neurons of the mouse brain. *J. Neurosci. Methods* **143**, 27-32. doi:10.1016/j.jneumeth.2004.09.020